SNOW COVER

VISIBLE/INFRARED IMAGER/RADIOMETER SUITE ALGORITHM THEORETICAL BASIS DOCUMENT

Version 5: March, 2002

Kenneth A. Jensen
Igor Appel

Science Team Members:
Dr. Eric Vermote, University of Maryland (Phase II)
Dr. Knut Stamnes, Stevens Institute of Technology (Phase I)
Dr. William Emery, University of Colorado

RAYTHEON SYSTEMS COMPANY
Information Technology and Scientific Services
4400 Forbes Boulevard
Lanham, MD 20706

SRBS Document # Y2401

EDR: Snow Cover

Doc No: Y2401

Version: 5

Revision: 0

	FUNCTION	NAME	SIGNATURE	DATE
PREPARED BY	EDR DEVELOPER	K. JENSEN		
APPROVED BY	SNOW/ICE IPT LEAD	K. JENSEN		
REVIEWED BY	REVIEWER	D. HOMMEL		
APPROVED BY	CHIEF SCIENTIST	S. MILLER		
RELEASED BY	ALGORITHM IPT LEAD	P.KEALY		

TABLE OF CONTENTS

Page

TABLE OF CONTENTS i

LIST OF FIGURES iii

LIST OF TABLES v

GLOSSARY OF ACRONYMS vi

ABSTRACT viii

1.0 INTRODUCTION 1
- 1.1 PURPOSE 1
- 1.2 SCOPE 1
- 1.3 VIIRS DOCUMENTS 1
- 1.4 REVISIONS 2

2.0 EXPERIMENT OVERVIEW 3
- 2.1 OBJECTIVES OF THE SNOW COVER RETRIEVAL 3
- 2.2 INSTRUMENT CHARACTERISTICS 5
- 2.3 ALGORITHM HERITAGE 9
  - 2.3.1 NOAA/TIROS 9
  - 2.3.2 DMSP 9
  - 2.3.3 Landsat 9
  - 2.3.4 NASA/EOS 9
- 2.4 RETRIEVAL STRATEGY 10
  - 2.4.1 Snow Binary Map 10
  - 2.4.2 Snow Fraction 10
  - 2.4.3 Snow Depth 11
  - 2.4.4 Snow Albedo 11

3.0 ALGORITHM DESCRIPTION 13
- 3.1 PROCESSING OUTLINE 13
- 3.2 ALGORITHM INPUT 16
  - 3.2.1 VIIRS Data 16
  - 3.2.2 Non-VIIRS Data 19
- 3.3 THEORETICAL DESCRIPTION OF THE RETRIEVAL 20

3.3.1 Physics of the Problem 20
3.3.2 Mathematical Description of the Snow Binary Map Algorithm 22
3.3.2.1 Correction for Directional Reflectance 25
3.3.3 Mathematical Description of the Snow Fraction Algorithm 26
3.3.3.1 Correction for Directional Reflectance 28
3.3.3.2 Endmember Selection (Non-snow Reflectance) 29
3.3.3.3 Snow Reflectance 29
3.3.3.4 Atmosphere / BRDF Coupling 30
3.3.4 Archived Algorithm Output 30
3.3.5 Algorithm Watch List 30
3.3.5.1 Surface Directional Effects 30
3.3.5.2 Snow Cover 31
3.3.5.3 Impact of Cloud Mask 32

4.0 EDR PERFORMANCE 33
4.1 STRATIFICATION 33
4.1.1 Snow Binary Map 33
4.1.2 Snow Fraction 34
4.2 STRATIFIED PERFORMANCE ANALYSIS 34
4.2.1 Snow Binary Map 34
4.2.1.1 Snow Binary Map Error Budgets 48
4.2.2 Snow Fraction 48
4.2.2.1 Snow Fraction Error Budget 51
4.3 LIMITS OF APPLICABILITY 51
4.3.1 Cloudy 51
4.3.2 Low Light or Nighttime 52
4.3.3 Forest Canopy (snow fraction) 52
4.4 PRACTICAL CONSIDERATIONS 52
4.4.1 Numerical Computation Considerations 52
4.4.2 Programming and Procedural Considerations 52
4.4.3 Configuration of Retrievals 53
4.4.4 Quality Assessment and Diagnostics 53
4.4.5 Exception Handling 53
4.5 VALIDATION 54

5.0 ASSUMPTIONS 57

6.0 REFERENCES 59

LIST OF FIGURES

Page

Figure 1. Summary of VIIRS design concepts and heritage 6

Figure 2. VIIRS detector footprint aggregation scheme for building Imagery "pixels". 6

Figure 3. Horizontal Sampling Interval (HSI) for imagery bands..... 7

Figure 4. Process flow for the Snow Cover EDR algorithm 13

Figure 5. Representative reflectance spectra for snow, vegetation, soil, and water (from Klein, Hall, and Riggs, 1998). 21

Figure 6. Representative reflectance spectra for snow and clouds (from Hall et al., 1998)..... 21

Figure 7. Near-Infrared Reflectance versus NDSI plot for winter and summer Landsat TM scenes of Glacier National Park, Montana (from Hall et al., 1998). Pixels located in the cross-hatched region are classified as snow. Winter forest pixels, which are known to have snow cover under the forest canopy, are incorrectly classified as no snow. 23

Figure 8. NDSI versus NDVI plot for modeled aspen, jack pine, and spruce stands (from Klein, Hall, and Riggs, 1998). The hatched region is the snow classification region for the Version 4 MODIS algorithm. The gray shaded region represents a proposed additional region for capturing snow-covered forests..... 24

Figure 9. (a) Visible reflectance image of Death Valley scene from MAS/SUCCESS campaign. The grey-scale is from 0.0 to 0.5 in reflectance. (b) Short Wave IR reflectance image of the scene. The grey-scale is from 0.0 to 0.5 in reflectance. 36

Figure 10. NDSI versus NDVI scatter plot of the MAS Death Valley scene (SUCCESS_115_16). The image has been aggregated to a VIIRS pixel size at nadir 37

Figure 11. (a) Visible reflectance image of Brazil scene from MAS/SCAR-B campaign. The color scale is from 0.0 to 0.2 in reflectance. (b) NDVI image of the scene. The color scale is from 0.05 to 0.7 in NDVI units. (c) NDSI image of the scene. The color scale is from -0.5 to 0.07 in NDSI units..... 38

Figure 12. NDSI versus NDVI scatter plot of the MAS Brazil scene (SCAR-B_163_1). The image has been aggregated to a VIIRS pixel size at nadir 39

Figure 13. (a)Visible reflectance image of Minnesota winter scene from MAS/WINCE campaign. The grey-scale is from 0.0 to1.0 in reflectance. (b) Normalized Difference Snow Index (NDSI) image of the scene. The color scale is from NDSI = 0.0 (darkest) to NDSI = 0.8. (c) Normalized Difference Vegetation Index (NDVI) image of the scene. The color scale is reversed, from NDVI = 0.25 (darkest) to NDVI = 0.05..... 40

Figure 14. NDSI versus NDVI scatter plot of the MAS Minnesota winter scene (WINCE_49_06). The image has been aggregated to a VIIRS pixel size at nadir. 41

Figure 15. (a) Visible Reflectance at 50 meter resolution, taken from a 0.648 micron image of Eastern Colorado obtained by the MODIS Airborne Simulator (MAS) on February 13, 1997. The extent of the scene is 35 km x 100 km. (b) Snow fraction at 0.4 km resolution, obtained by classification and aggregation to a VIIRS pixel size at nadir. (c) Retrieved Binary Snow Cover map. System performance errors were used to simulate a VIIRS retrieval. Green cells are mapped as snow. 97.8 % of the pixels were correctly typed..... 42

Figure 16. NDSI versus NDVI scatter plot of the MAS Colorado winter scene (WINCE_50_14). The image has been aggregated to a VIIRS pixel size at nadir. 43

Figure 17. NDSI versus NDVI scatter plot of the MAS Colorado winter scene (WINCE_50_14). The image has been aggregated to a VIIRS pixel size at nadir. Error perturbations have been added to the scene. 44

Figure 18. Probability of Correct Typing vs. Snow Fraction for the MAS Colorado winter scene (WINCE_50_14). The scene was aggregated to a pixel size of 0.4 km to simulate a VIIRS nadir view. 45

LIST OF TABLES

Page

Table 1. Specifications of the VIIRS Snow Cover (Binary Map) EDR 3

Table 2. Specifications of the VIIRS Snow Cover (Snow Fraction) EDR 4

Table 3. Snow Binary Map Algorithm – Input Data Summary 7

Table 4. Snow Fraction Algorithm – Input Data Summary 8

Table 5. VIIRS Data for the VIIRS Snow Cover Algorithms 16

Table 6. Snow Binary Map : Probability of Correct Typing (%) 45

Table 7. Error Budget for Retrieval of the Snow Binary Map EDR (Case 1) 46

Table 8. Error Budget for Retrieval of the Snow Binary Map EDR (Case 2) 47

Table 9. Error Budget for Retrieval of the Snow Binary Map EDR (Case 3) 47

Table 10. Snow Fraction Measurement Uncertainty : Clear, 10% Mixed Pixels (Easy case) 50

Table 11. Snow Fraction Measurement Uncertainty : Clear, 30% Mixed Pixels (Typical case) 50

Table 12. Snow Fraction Measurement Uncertainty : Clear, 50% Mixed Pixels (Hard case) 50

Table 13. Error Budget for Retrieval of the Snow Fraction EDR 51

GLOSSARY OF ACRONYMS

AOT	Aerosol Optical Thickness
AMSR	Advanced Microwave Scanning Radiometer
ARF	Anisotropic Reflectance Factor
ATBD	Algorithm Theoretical Basis Document
AVHRR	Advanced Very High Resolution Radiometer
AVIRIS	Airborne Visible/Infrared Imaging Spectrometer
BRDF	Bidirectional Reflectance Distribution Function
BRF	Bidirectional Reflectance Function
CDR	Critical Design Review
CMIS	Conical Scanning Microwave Imager/Sounder
DAAC	Distributed Active Archive Center
DISORT	Discrete Ordinates Radiative Transfer
DMSP	Defense Meteorological Satellite Program
DoD	Department of Defense
EDR	Environmental Data Record
ENVI	Environment for Visualizing Images
EOS	Earth Observing System
GCM	General Circulation Model
GIFOV	Ground Instantaneous Field of View
GLI	Global Imager
GSD	Ground Sample Distance
HCS	Horizontal Cell Size
HSI	Horizontal Sampling Interval
HSR	Horizontal Spatial Resolution
IP	Intermediate Product
JHU	Johns Hopkins University
LLLS	Low-Level Light Sensor
LUT	Look-Up Table
MAS	MODIS Airborne Simulator
MESMA	Multiple Endmember Spectral Mixture Analysis
MODIS	Moderate Resolution Imaging Spectroradiometer
MSS	Multispectral Scanner
MTF	Modulation Transfer Function
NASA	National Aeronautics and Space Administration
NASA/GSFC	NASA/Goddard Space Flight Center
NDSI	Normalized Difference Snow Index

NDVI	Normalized Difference Vegetation Index
NESDIS	National Environmental Satellite, Data and Information Service
NIR	Near Infrared
NOAA	National Oceanic and Atmospheric Administration
NOHRSC	National Operational Hydrologic Remote Sensing Center
NPOESS	National Polar-orbiting Operational Environmental Satellite System
NPP	NPOESS Preparatory Program
OLS	Operational Linescan System
P^3I	Pre-Planned Product Improvement
PDR	Preliminary Design Review
RDR	Raw Data Record
RMS	Root Mean Square
RT	Radiative Transfer
SCAR-B	Smoke, Clouds, and Radiation - Brazil
SDR	Sensor Data Record
SMA	Spectral Mixture Analysis
SRD	Sensor Requirements Document
SSM/I	Special System Microwave/Imager
SUCCESS	Subsonic Aircraft Contrail and Cloud Effects Special Study
SWE	Snow-Water Equivalent
SWIR	Short Wave Infrared
SZA	Solar Zenith Angle
TBD	To Be Determined
TBR	To Be Reviewed
TBS	To Be Specified
THEMIS	Thermal Emission Imaging System
TIROS	Television Infrared Observing System
TM	Thematic Mapper
TOA	Top-of-Atmosphere
VIIRS	Visible/Infrared Imager/Radiometer Suite
VIS	Visible
VIS/IR	Visible/Infrared
VOAT	VIIRS Operational Algorithm Team
WINCE	Winter Cloud Experiment

ABSTRACT

The following document is version 5 of the Algorithm Theoretical Basis Document (ATBD) for Snow Cover retrieval from surface reflectances. The reflectances are to be derived from Top-of-Atmosphere (TOA) radiances received by the National Polar-orbiting Operational Environmental Satellite System (NPOESS) Visible/Infrared Imager/Radiometer Suite (VIIRS). Snow Cover, a VIIRS level 2 product, is one of the required VIIRS Environmental Data Records (EDRs) as stated in the VIIRS Sensor Requirements Document (SRD). The surface reflectances will be supplied as a VIIRS Intermediate Product (IP), as documented in the VIIRS Surface Reflectance ATBD *[Y2411]*. The purpose of this document is to describe the theoretical basis and development process of the algorithms to retrieve a binary snow/no snow map and the fraction of snow cover in a specified horizontal cell, as required by the VIIRS SRD.

The VIIRS Snow Cover EDR threshold requirement is that a binary snow/no snow map be produced at a horizontal cell size of 0.5 km at nadir under clear, daytime conditions, with a probability of correct typing of 90% or better. The algorithm to retrieve the binary map uses the surface reflectance in three VIIRS imagery resolution reflectance bands. It is an adaptation of the Moderate Resolution Imaging Spectroradiometer (MODIS) snow algorithm, which classifies a pixel as snow or no snow from its values of Normalized Difference Snow Index (NDSI) and Normalized Difference Vegetation Index (NDVI). The VIIRS algorithm uses a red band in place of the green band used by the MODIS algorithm, allowing us to achieve imagery resolution (0.4 km at nadir). Our analysis shows that the red band NDSI threshold is nearly identical to the green band NDSI threshold. Our performance analysis leads to a performance estimate of 95% or better probability of correct typing for most cases, consistent with the expected performance of the MODIS algorithm. The algorithm, which will benefit directly from MODIS heritage, is a low risk approach with the capability of providing an operational, global snow cover product.

The VIIRS Snow Cover EDR objective requirement is that the horizontal extent of snow cover be retrieved globally at a horizontal cell size of 1.3 km under clear, daytime conditions. The measurement range will be the fraction of snow cover from 0 to 1, with a measurement uncertainty of 0.1. The algorithm to retrieve snow fraction uses the surface reflectance in nine VIIRS moderate resolution reflectance bands. The algorithm is an application of Multiple Endmember Spectral Mixture Analysis (MESMA). An objective of any spectral mixture analysis is the definition of subpixel proportions of spectral endmembers that may be related to mappable surface constituents. Spectral mixture analysis “unmixes” the mixed pixel, determining the fractions of each spectral endmember which combine to produce the mixed pixel’s spectral signature. Our approach is to model the signature from each pixel as a combination of two components: a modeled snow reflectance spectrum and a modeled non-snow reflectance spectrum. The approach is based on the assumption that the non-snow endmember spectrum for each pixel is sufficiently modeled by a monthly mean non-snow reflectance, acquired operationally from a VIIRS IP. Our performance analysis indicates that the measurement uncertainty requirement can be achieved, except for scenes with forest canopy.

This document presents the algorithm theoretical basis, the input data requirements, the EDR performance specification and error analysis, conditions under which the specification can not be attained, and the plan for initialization and validation. It is a revision of the version 4 algorithm, which should be considered to be completely superseded by the new version. Changes since version 4 include the development of look up tables (LUTs) for snow reflectance, non-snow BDRF, pixel quality determination, and pixel/band weighting.

1.0 INTRODUCTION

1.1 PURPOSE

This Algorithm Theoretical Basis Document (ATBD) explains the mathematical background to derive the Snow Cover Environmental Data Record (EDR). This document also provides an overview of required input data, physical theory, assumptions, limitations, and a performance analysis of the described algorithms. The Snow Cover EDR is obtained from measurements of the National Polar-orbiting, Operational Environmental Satellite System (NPOESS) Visible/Infrared Imager/Radiometer Suite (VIIRS). The one EDR described in this document is part of the NPOESS/VIIRS team software package of EDRs.

1.2 SCOPE

This document covers the theoretical basis for the derivation of the Snow Cover EDR, which consists of a binary snow/no snow map and snow fraction in a horizontal cell. The purpose and scope of the document are described in Section 1, while Section 2 provides an overview of the snow cover retrieval objectives. Section 3 describes the algorithm, its input data, the theoretical background, and some practical considerations. Section 4 contains the EDR performance analysis and error budget. Section 5 contains the pre-launch and post-launch plan for verification and validation. Section 6 contains assumptions and limitations.

1.3 VIIRS DOCUMENTS

This document contains references to other Raytheon VIIRS documents, designated by a document number, which is given in italicized brackets. The VIIRS documents cited in this document are:

[SS 154640-001] - VIIRS System Specification

[PS 154640-101] - VIIRS Sensor Specification

[TP 154640-001] - VIIRS System Verification and Validation Plan Document

[TP 154640-118] - VIIRS Radiometric Calibration and Validation Plan

[Y2400] - VIIRS Vegetation Index ATBD

[Y2411] - VIIRS Surface Reflectance ATBD

[Y2412] - VIIRS Cloud Mask ATBD

[Y2468] - VIIRS Operations Concept document

[Y2469] - VIIRS Context Level Software Architecture

[Y2470] - VIIRS Interface Control Document

[Y2471] - VIIRS Aerosol Module Level Software Architecture

[Y2472] - VIIRS Cloud Module Level Software Architecture

[Y2477] - VIIRS Snow Ice Module Level Software Architecture

[Y2478] - VIIRS Build-RDR Module Level Software Architecture Document

[Y2479] - VIIRS Build SDR Module Level Software Architecture

[Y3234] - VIIRS Snow Cover Unit Level Detailed Design Document

[Y3236] - VIIRS Software Integration and Test Plan

[Y3237] - VIIRS Algorithm Verification and Validation Plan

[Y3258] - VIIRS Geolocation ATBD

[Y3261] - VIIRS Radiometric Calibration ATBD

[Y3270] - VIIRS System Verification and Validation Plan

[Y3277] - VIIRS Aerosol Module Level Interface Control Document

[Y3278] - VIIRS Cloud Module Level Interface Control Document

[Y6635] - VIIRS Algorithm Software Development Plan.

[*Y6661]* - VIIRS Algorithm Software Maturity Assessment document

[Y7040] - VIIRS Algorithm/Data Processing Technical Report

[Y10810] - VIIRS Look up Table Generation Tool (LUTGT) Detailed Design Document

1.4 REVISIONS

This is the fifth version of this document, dated March 2002. Version 5.0 is released as part of the Raytheon NPOESS/VIIRS Critical Design Review (CDR) package. The first two versions were developed in response to VIIRS Sensor Requirements Document (SRD), revision 1, dated August 3, 1998. The first version was dated October 1998. The second version was dated June 1999. The third version, dated May 2000, was developed in response to VIIRS Sensor Requirements Document (SRD), Version 2, Revision a, dated 04 November 1999 and was submitted as part of the Raytheon NPOESS/VIIRS Preliminary Design Review (PDR) and Proposal packages.

The primary purpose of version 4 was to respond to VIIRS Algorithm Watch List items generated by the VIIRS Operational Algorithm Team (VOAT). An additional purpose was to incorporate minor revisions generated by an internal Raytheon review since the VIIRS PDR. Changes since version 3 included:

- Inclusion of Bidirectional Reflectance Distribution Function (BRDF) correction factors
- Expanded description of input data, including VIIRS gridded data
- Revision and enhancement of the process flow description
- Responses to relevant VOAT Watch List Items and other reviewer comments

This document, version 5.0, incorporates the post-PDR developments in software architecture and detailed design that bring the algorithm to a CDR level of maturity. Changes since version 4 include:

- Additional development of the algorithm, with a detailed process flow and description of the LUTs.
    - The introduction of a process that performs pixel masking and pixel weighting

2.0 EXPERIMENT OVERVIEW

2.1 OBJECTIVES OF THE SNOW COVER RETRIEVAL

Because of its high albedo, snow is an important factor in determining the radiation balance, with implications for global climate studies (Foster and Chang, 1993). General circulation models (GCM) do not simulate the Arctic climate very well (Bromwich and Tzeng, 1994), indicating the need to improve measurements of the global snow cover. Weekly snow cover maps of the Northern Hemisphere have been produced since 1966 by the National Oceanic and Atmospheric Administration (NOAA: Matson, Roeplewski, and Varnadore, 1986; Matson, 1991). Daily and 8-day composite global maps are an objective of the recently launched National Aeronautics and Space Administration (NASA) Moderate Resolution Imaging Spectroradiometer (MODIS) instrument (Hall et al., 1998). Regionally, the measurement of snowpack properties is vital to the prediction of water supply and flood potential (Carroll *et al.*, 1989; Chang *et al.*, 1987). Regional snow products with 1 km resolution are produced by the National Weather Service (Carroll, 1990), and are expected at 500 meter resolution from MODIS. The objective of the VIIRS retrieval is to achieve the performance specifications designed to meet the requirements stated in the VIIRS Sensor Requirements Document (SRD). These are given in Table 1 (Binary map) and Table 2 (Snow fraction).

Table 1. Specifications of the VIIRS Snow Cover (Binary Map) EDR

Parameter	Thresholds	Objectives	Specification Value
a. Horizontal Cell Size,			
1. Clear – daytime (Worst case)	1.3 km (TBR)	N/A	0.8 km
2. Clear – daytime (At nadir)	0.5 km (TBR)	N/A	0.4 km
3. Cloudy and/or nighttime	12.5 km	N/A	NPOESS / CMIS*Capability
b. Horizontal Reporting Interval	(TBD)	N/A	Horizontal Cell Size
c. Snow Depth Ranges	> 0 cm (Any Snow Thickness)	N/A	> 0 cm (Any Snow Thickness)
d. Horizontal Coverage	Land	N/A	Land
e. Vertical Coverage	> 0 cm	N/A	> 0 cm
f. Measurement Range	Snow / No snow	N/A	Snow / No snow
g. Probability of Correct Typing(Clear – daytime)	90% (TBR) at (TBS)% confidence level	N/A	95%
h. Mapping Uncertainty, Clear	3 km	N/A	0.133 km (nadir)
m. Minimum Swath Width	3000 km (TBR)	N/A	3000 km

* Conical-Scanning Microwave Imager/Sounder

Table 2. Specifications of the VIIRS Snow Cover (Snow Fraction) EDR

Parameter	Thresholds	Objectives	Specification Value
a. Horizontal Cell Size,			
1. Clear – daytime (Worst case)	1.3 km (TBR)	1 km	1.6 km
2. Clear – daytime (At nadir)	N/A	N/A	0.8 km
3. Cloudy and/or nighttime	12.5 km	1 km	NPOESS / CMIS Capability
b. Horizontal Reporting Interval	(TBD)	(TBD)	Horizontal Cell Size
c. Snow Depth Ranges	> 0 cm (Any Snow Thickness)	> 0 cm (Any Snow Thickness)	> 0 cm (Any Snow Thickness)
d. Horizontal Coverage	Land	Land & Ice	Land
e. Vertical Coverage	> 0 cm	> 0 cm	> 0 cm
f. Measurement Range	N/A	0 – 1	0 – 1
n. Measurement Uncertainty (Clear – daytime)	N/A	10%	0.1
h. Mapping Uncertainty, Clear	3 km	1 km	0.5 km (worst case)
m. Minimum Swath Width	3000 km (TBR)	(TBD)	3000 km
Units: Dimensionless			

The specifications apply under clear, daytime conditions only. Surface properties can not be observed through cloud cover by a Visible/Infrared (VIS/IR) sensor.

2.2 INSTRUMENT CHARACTERISTICS

The VIIRS instrument can be pictured as a convergence of three existing sensors, two of which have seen extensive operational use at this writing.

The Operational Linescan System (OLS) is the operational visible/infrared scanner for the Department of Defense (DoD). Its unique strengths are controlled growth in spatial resolution through rotation of the ground instantaneous field of view (GIFOV) and the existence of a low-level light sensor (LLLS) capable of detecting visible radiation at night. OLS has primarily served as a data source for manual analysis of imagery. The Advanced Very High Resolution Radiometer (AVHRR) is the operational visible/infrared sensor flown on the National Oceanic and Atmospheric Administration (NOAA) Television Infrared Observation Satellite (TIROS-N) series of satellites (Planet, 1988). Its unique strengths are low operational and production cost and the presence of five spectral channels that can be used in a wide number of combinations to produce operational and research products. In December 1999, the National Aeronautics and Space Administration (NASA) launched the Earth Observing System (EOS) morning satellite, *Terra*, which includes the Moderate Resolution Imaging Spectroradiometer (MODIS). This sensor possesses an unprecedented array of thirty-two spectral bands at resolutions ranging from 250 m to 1 km at nadir, allowing for unparalleled accuracy in a wide range of satellite-based environmental measurements.

VIIRS will reside on a platform of the National Polar-orbiting Operational Environmental Satellite System (NPOESS) series of satellites. It is intended to be the product of a convergence between DoD, NOAA and NASA in the form of a single visible/infrared sensor capable of satisfying the needs of all three communities, as well as the research community beyond. As such, VIIRS will require three key attributes: high spatial resolution with controlled growth off nadir, minimal production and operational cost, and a large number of spectral bands to satisfy the requirements for generating accurate operational and scientific products.

The VIIRS sensor specification is based on the sensor requirements of the National Polar-orbiting Operational Environmental Satellite System (NPOESS) and on EDR thresholds and objectives. The Snow Cover algorithm takes as input geolocated, calibrated Sensor Data Records (SDRs) generated from three VIIRS Imagery bands and nine VIIRS moderate resolution bands *[Y2478]*. The SDRs are obtained from VIIRS RDRs by an RDR to SDR process. The RDRs are obtained by a rotating telescope scanning mechanism that minimizes the effects of solar impingement and scattered light. Figure 1 illustrates the design concept for VIIRS, designed and built by Raytheon Santa Barbara Remote Sensing (SBRS). VIIRS is essentially a combination of SeaWiFS foreoptics and an all-reflective modification of MODIS/THEMIS aft-optics. Calibration is performed onboard using a solar diffuser for short wavelengths and a blackbody source and deep space view for thermal wavelengths. A solar diffuser stability monitor (SDSM) is also included to track the performance of the solar diffuser. The VIIRS scan will extend to 56 degrees on either side of nadir, providing a swath of 3000 km for the nominal satellite altitude of 833 km.

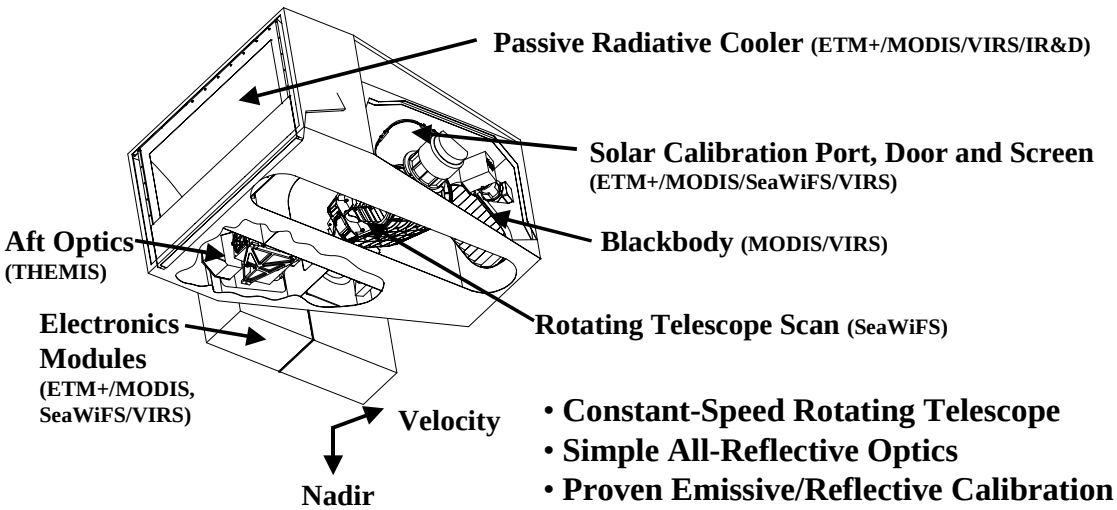

Figure 1. Summary of VIIRS design concepts and heritage.

The VIIRS SRD places explicit requirements on spatial resolution for the Imagery EDR. Specifically, the horizontal spatial resolution (HSR) of bands used to meet threshold Imagery EDR requirements must be no greater than 400 m at nadir and 800 m at the edge of the scan. This led to the development of a unique scanning approach which optimizes both spatial resolution and signal to noise ratio (SNR) across the scan. The concept is summarized in Figure 2 for the imagery (fine resolution) bands. The VIIRS detectors are rectangular, with the smaller dimension along the scan. At nadir, three detector footprints are aggregated to form a single VIIRS "pixel." Moving along the scan away from nadir, the detector footprints become larger both along track and along scan, due to geometric effects and the curvature of the Earth. The effects are much larger along scan. At 31.59 degrees in scan angle, the aggregation scheme is changed from 3x1 to 2x1. A similar switch from 2x1 to 1x1 aggregation occurs at 44.68 degrees. The VIIRS scan consequently exhibits a pixel growth factor of only 2 both along track and along scan, compared with a growth factor of 6 along scan which would be realized without the use of the aggregation scheme. This scanning approach allows VIIRS to provide imagery at 800-m resolution or finer globally, with 375-m resolution at nadir. Additionally, due to the imagery requirements for VIIRS and the "sliver" detector design, MTF performance will be extremely sharp (0.5 at Nyquist).

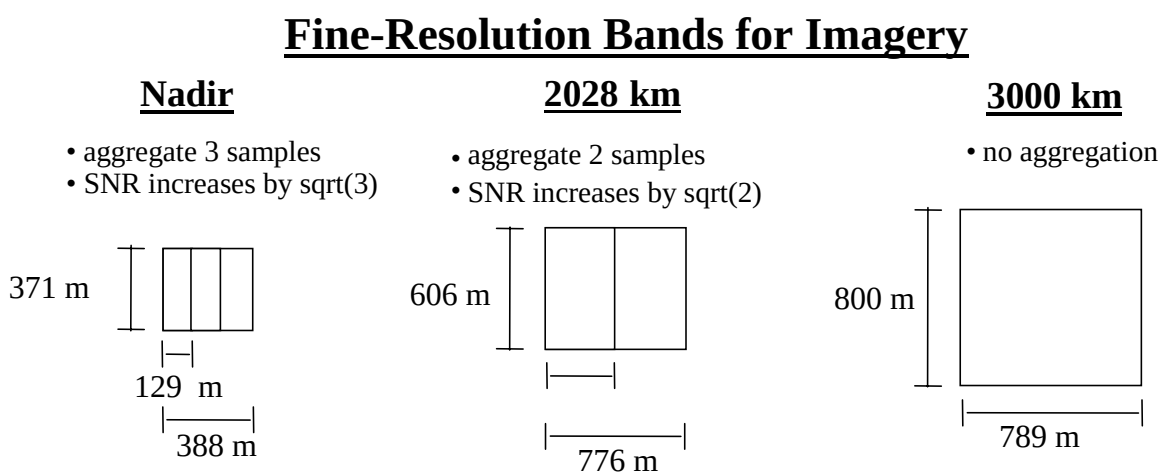

Figure 2. VIIRS detector footprint aggregation scheme for building Imagery "pixels".

Figure 3, showing the Horizontal Sampling Interval (HSI) that results from the combination scan/aggregation scheme, illustrates the benefits of the aggregation scheme for spatial resolution.

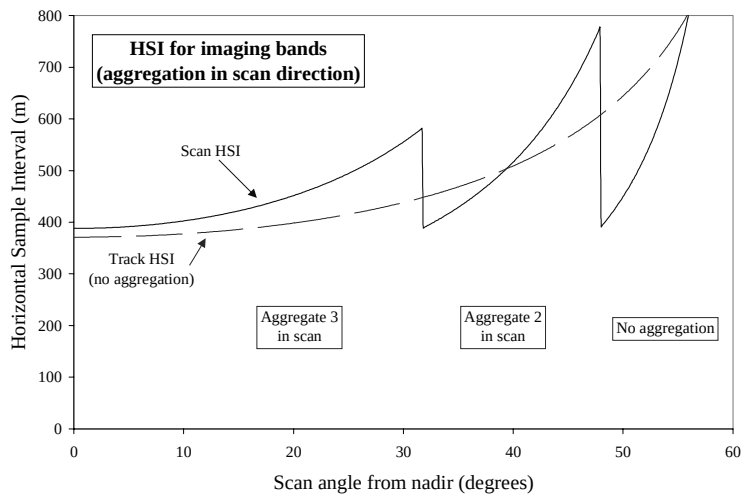

Figure 3. Horizontal Sampling Interval (HSI) for imagery bands (aggregation in scan direction).

The aggregation switch points occur at scan angles of 31.59 degrees (3 to 2 aggregation) and 44.68 degrees (2 to no aggregation).

The VIIRS Snow Cover EDR benefits greatly from the high performance requirements placed on the VIIRS Imagery EDR, as the algorithm uses the imagery bands for input data. The performance characteristics of the bands used by the Snow Cover algorithm, listed in Table 3 and Table 4, are obtained from the VIIRS Sensor Specification Document *[PS 154640-101]* and the VIIRS Radiometric Calibration ATBD *[Y3261]*. The VIIRS sensor has been designed from the NPOESS sensor requirements and the flowdown of EDR requirements. Complete details on the instrument design are provided in the Raytheon VIIRS Sensor Specification Document *[PS154640-101]*.

The binary map algorithm uses surface reflectance in three bands at imagery resolution. Table 3 lists the characteristics of these bands.

Table 3. Snow Binary Map Algorithm – Input Data Summary

VIIRS Band	$\lambda(\mu m)$	$\Delta\lambda(\mu m)$	GSD* (m) at Nadir (Track x Scan)	HCS** (m) at Nadir (Track x Scan)	GSD (m) at Edge of Scan (Track x Scan)	HCS (m) at Edge of Scan (Track x Scan)
I1	0.645	0.080	371 x 131	371 x 393	800 x 800	800 x 800
I2	0.865	0.039	371 x 131	371 x 393	800 x 800	800 x 800
I3	1.61	0.060	371 x 131	371 x 392	800 x 800	800 x 800

* - Ground Sample Distance ** - Horizontal Cell Size

Each band has a calibration accuracy specification of 2%. The expected band noise performance provides signal-to-noise better than 100 for most cases *[PS154640-101]*.

The snow fraction algorithm uses surface reflectance in 9 bands at moderate resolution. This is a change from Version 3, which also used the three imagery resolution reflectance bands. We have eliminated the imagery resolution bands from the algorithm for the following reasons:

1) Because the modulation transfer functions (MTFs) of the imagery resolution bands are not directly scaleable by a factor of 2 compared with the MTFs of the radiometric bands, the 2 x 2 aggregation of imagery bands introduces an MTF mismatch with the radiometric bands.

2) The added complexity of MTF matching is not warranted by the limited additional spectral information in the imagery bands, as the performance of spectral mixture analysis will level off asymptotically as additional bands are added.

Table 4 lists the characteristics of the 9 bands used in the snow fraction algorithm.

Table 4. Snow Fraction Algorithm – Input Data Summary

VIIRS Band	$\lambda(\mu m)$	$\Delta\lambda(\mu m)$	GSD (m) at Nadir (Track x Scan)	HCS (m) at Nadir (Track x Scan)	GSD (m) at Edge of Scan (Track x Scan)	HCS (m) at Edge of Scan (Track x Scan)
M1	0.410	0.020	742 x 262	742 x 786	1600 x 1600	1600 x 1600
M2	0.445	0.018	742 x 262	742 x 786	1600 x 1600	1600 x 1600
M3	0.488	0.020	742 x 262	742 x 786	1600 x 1600	1600 x 1600
M4	0.555	0.020	742 x 262	742 x 786	1600 x 1600	1600 x 1600
M5	0.672	0.020	742 x 262	742 x 786	1600 x 1600	1600 x 1600
M7	0.865	0.039	742 x 262	742 x 786	1600 x 1600	1600 x 1600
M8	1.24	0.020	742 x 262	742 x 786	1600 x 1600	1600 x 1600
M10	1.61	0.060	742 x 262	742 x 786	1600 x 1600	1600 x 1600
M11	2.25	0.050	742 x 262	742 x 786	1600 x 1600	1600 x 1600

Each band has a calibration accuracy specification of 2%. The expected band noise performance provides signal-to-noise better than 100 for most cases *[PS154640-101]*.

2.3 ALGORITHM HERITAGE

2.3.1 NOAA/TIROS

Initially, the weekly NOAA National Environmental Satellite Data and Information System (NESDIS) operational product was determined from visible satellite imagery from polar-orbiting and geostationary satellites and surface observations. The analysis was performed once a week, using the most recent clear view of the surface. Because the analysis for this product was done only once a week, much snow cover, especially from fleeting/transient storms, was missed. Where cloud cover precluded the analyst's view of the surface for an entire week, the analysis from the previous week was carried forward (Ramsay, 1998). The maps were hand drawn, and then digitized using an 89 X 89 line grid overlaid on a stereographic map of the Northern Hemisphere. In 1997, the older, weekly maps were replaced in 1997, by the IMS product. The IMS product provides a daily snow map that is constructed through the use of a combination of techniques including visible, near-infrared and passive-microwave imagery and meteorological-station data at a spatial resolution of about 25 km (Ramsay, 1998 and 2000).

Regional snow products, with 1-km resolution, are produced operationally in 3000 - 4000 drainage basins in North America by the National Weather Service using NOAA National Operational Hydrologic Remote Sensing Center (NOHRSC) data (Carroll, 1990 and Rango, 1993).

2.3.2 DMSP

Passive-microwave sensors on-board the Nimbus 5, 6, and 7 satellites and the Defense Meteorological Satellite Program (DMSP) have been used successfully for measuring snow extent at a 25- to 30-km resolution through cloud-cover and darkness since 1978 (Chang et al., 1987). Passive-microwave sensors also provide information on global snow depth (Foster et al., 1984).

2.3.3 Landsat

The Landsat Multispectral Scanner (MSS) and TM sensors, with 80-m and 30-m resolution, respectively, are useful for measurement of snow covered area over drainage basins (Rango and Martinec, 1982). Additionally, Landsat TM data are useful for the quantitative measurement of snow reflectance (Dozier et al., 1981; Dozier, 1984 and 1989; Hall et al., 1989; Winther, 1992).

2.3.4 NASA/EOS

The launch of the EOS Terra satellite in December 1999 introduced a new era in global snow mapping. The MODIS Level-3 products will include daily and 8-day composites of global snow cover at 500-m resolution. Statistics will be provided regarding the extent and persistence of snow cover at each grid cell for the Level-3 products. These products are produced from the MODIS Level-2 snow product, which is a swath-based binary snow/no snow map, derived by the MODIS snow-mapping algorithm (Snowmap; Hall et al., 1998, 2001a). Our snow algorithm, discussed in Section 3, draws heavily from the MODIS algorithm.

Advanced Microwave Scanner Radiometer (AMSR)-derived snow and ice maps will be available following the launch of the EOS Aqua satellite. Algorithms will be developed that will employ both MODIS and AMSR data to map snow cover and depth. It is envisioned that a product can be developed that will employ reflective and passive-microwave data that will permit snow extent, albedo and depth to be mapped, thus enabling daily maps to be generated irrespective of cloud cover and darkness. The MODIS/AMSR data will be very useful in the

development of a prospective NPOESS pre-planned product improvement (P^3I) for snow cover/depth, using VIIRS/CMIS data.

2.4 RETRIEVAL STRATEGY

2.4.1 Snow Binary Map

The input data will consist of a two-dimensional grid of surface pixels for each of three VIIRS imagery resolution bands in the form of geolocated surface reflectances. Surface reflectances will be supplied as a required Surface Reflectance IP for the Surface Albedo EDR, as documented in the Surface Reflectance ATBD *[Y2411]*.

The Cloud Mask algorithm *[Y2412]* will identify pixels that should be excluded from processing due to cloud or cloud shadow. The Cloud Mask will also supply a land/water mask.

Each pixel will be examined for its suitability. Pixels designated as land by the land/water mask and as “clear” or “probably clear” by the cloud mask will be passed for processing. Pixels designated as “probably clear” will have a quality flag attached to them. The solar/sensor angles for each pixel will be used to determine whether the pixel is rejected, passed for further processing with a quality flag attached, or passed for further processing without reservation.

Pixels which have been passed for processing will have their values of NDSI, NDVI, and NIR reflectance examined to determine a snow or no snow classification, following the prescription described in Section 3.3.2.

Recent MODIS experience suggests that a thermal mask should be used to avoid snow classification from dense forest regions in the tropics (Barton, Hall, and Riggs 2001). Application of a threshold 11 micron brightness temperature of 277K screens out all pixels with greater surface temperature. It is probable that we will adopt this mask for our algorithm. In that case, the algorithm will also acquire the band M15 brightness temperature from the VIIRS EV_750M SDR.

The process flow to implement the snow binary map retrieval is outlined in Section 3.1.

2.4.2 Snow Fraction

The input data will consist of a two-dimensional grid of surface pixels for each of nine VIIRS moderate resolution bands in the form of geolocated surface reflectances. Surface reflectances will be supplied as a required Surface Reflectance IP for the Surface Albedo EDR, as documented in the Surface Reflectance ATBD *[Y2411]*. The snow fraction algorithm uses all available reflectance band information, on the assumption that the relative weight of each band can be determined (c.f. Section 3.3.3). If each band contained completely independent information, the algorithm variance would scale as 1/N, where N is the number of bands. Because reflectance spectra contain band correlations, actual performance will not improve as much. Our performance analysis for snow fraction (c.f. Section 4.2.2) adopts the assumption that the bands are all completely correlated. To the extent that different bands contain independent information, algorithm performance will improve.

The Cloud Mask algorithm *[Y2412]* will identify pixels that should be excluded from processing due to cloud or cloud shadow and will also supply a land/water mask. A Forest LUT *[Y3234]* will supply a mask to identify boreal forest pixels requiring special consideration.

Each pixel will be examined for its suitability. Pixels designated as land by the land/water mask and as clear or probably clear by the cloud mask will be passed for processing. Pixels designated as "forest" by the forest mask will have a quality flag attached to them. Pixels designated as "probably clear" or "thin cirrus" will be given a reduced pixel weight, and may have a quality flag attached to them. The solar/sensor angles, aerosol optical thickness, and cloud optical thickness for each pixel will be used to derive pixel quality and pixel weight for each band. These will determine whether the pixel is rejected, passed for further processing with a quality flag attached, or passed for further processing without reservation.

The algorithm will acquire pixel-by-pixel information about non-snow spectral signatures from a reference database indicating the surface properties for the relevant month. Initially, we expect the database to be derived from MODIS and the NPOESS Preparatory Program (NPP) VIIRS. As the NPOESS mission progresses, we expect the database to be modified by the VIIRS observations, and provided as a Monthly Non-Snow Reflectance IP. This IP, discussed in the VIIRS Surface Reflectance ATBD *[Y2411]*, will be provided on the standard VIIRS Earth grid by the VIIRS Earth Gridding algorithm *[Y7051]*.

For each pixel that has been passed for further processing, Multiple Endmember Spectral Mixture Analysis (MESMA) will be performed to derive snow fraction, following the prescription described in Section 3.3.3.

The process flow to implement snow fraction retrieval is outlined in Section 3.1.

2.4.3 Snow Depth

Snow depth is no longer a VIIRS EDR requirement. It is recognized that data fusion between high resolution snow cover from Vis/IR and snow depth at coarser resolution from passive microwave would improve the overall snow product. MODIS/AMSR studies can be used to investigate this possibility, and could serve as a precursor to an NPOESS Level 3 P^3I product. For the purposes of our algorithm development, however, we are required to produce a VIIRS Snow Cover EDR within an operational timeline that precludes the use of contemporaneous CMIS data. We have therefore deferred a consideration of a combined VIIRS/CMIS snow cover/depth product.

2.4.4 Snow Albedo

A snow albedo algorithm has been developed for MODIS (Klein 2001; Klein, Hall, and Nolin, 2001). The algorithm will complement existing MODIS products by providing albedo measurements for areas mapped as snow on a global daily basis by MODIS. MODIS experience will be of great benefit to our algorithm development, as the modeling of snow albedo is critical to our approach for BRDF correction (c.f. Sections 3.3.2.1 and 3.3.3.1).

3.0 ALGORITHM DESCRIPTION

3.1 PROCESSING OUTLINE

The Snow Cover EDR is retrieved by an automated algorithm. The process flow is implemented within the Snow/Ice Module by the independent testable Snow Cover software unit, as illustrated in Figure 4.

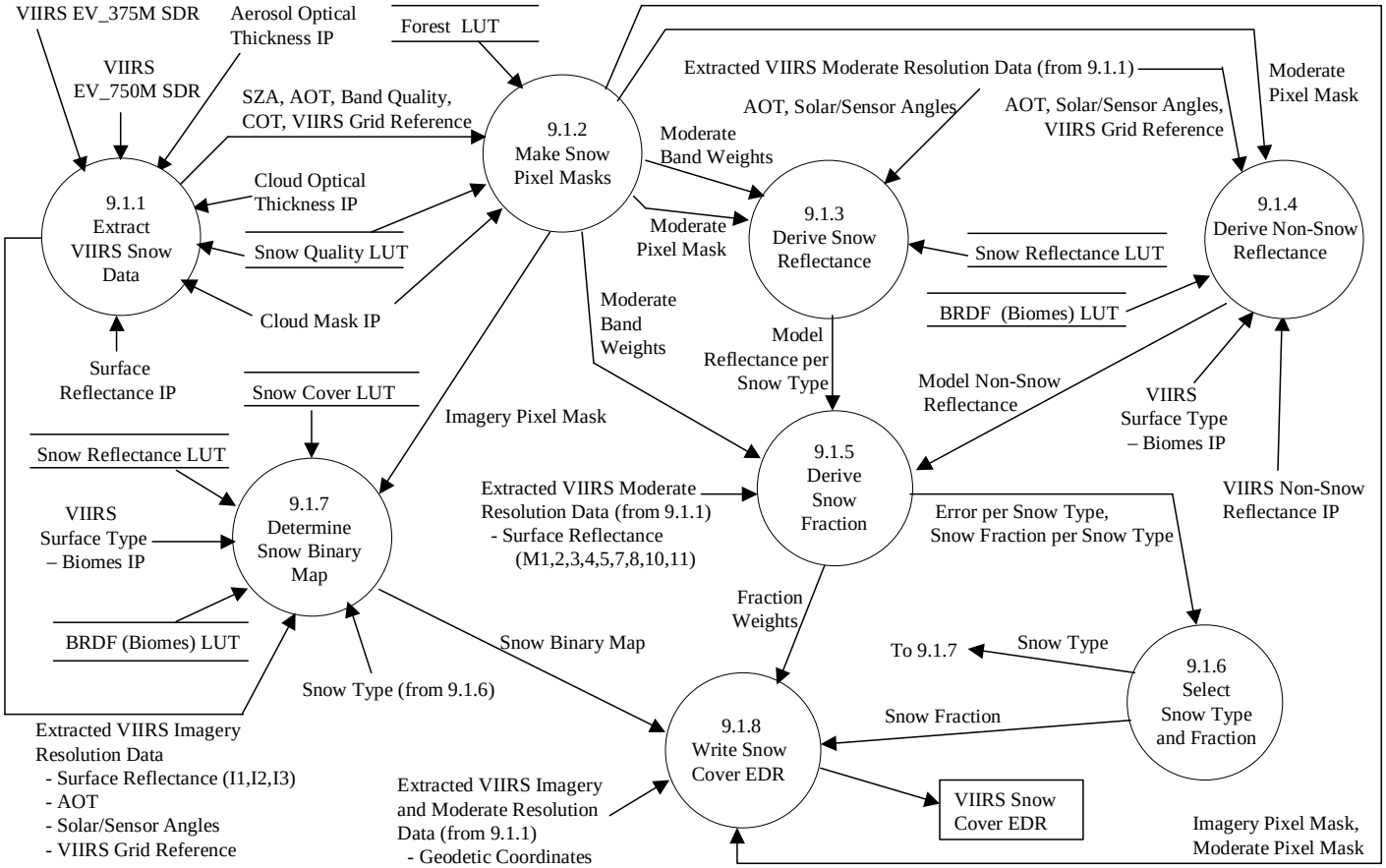

Figure 4. Process flow for the Snow Cover EDR algorithm.

The process flow is described in detail in the VIIRS Snow/Ice Module Level Software Architecture document *[Y2477]*. The main steps are as follows:

1) Input data for the current VIIRS granule is extracted by the *Extract VIIRS Snow Data* process. If all pixels are designated as Ocean in the Cloud Mask IP, processing is bypassed and a null EDR file is written.

2) The *Make Snow Pixel Masks* process *[Y3234]* performs pixel masking and pixel weighting, using information in the VIIRS EV_375M SDR *[Y2479]*, VIIRS Aerosol Optical Thickness IP *[Y2471]*, VIIRS Cloud Optical Thickness IP *[Y2479]*, VIIRS Cloud Mask IP *[Y2412]*, and a Snow Quality LUT *[Y3234]*. The process produces a pixel quality mask and pixel weights for each band.

3) Snow reflectance per snow type is modeled for each moderate resolution pixel by the *Derive Snow Reflectance* process. The process uses pre-set albedo and BRDF models for each snow type, obtained from the Snow Reflectance LUT, to derive expected direction reflectance for each of the nine moderate resolution bands used for snow fraction. Solar/sensor angles and AOT for each pixel are used to apply the BRDF. The following steps are implemented:

   a. Narrow band snow albedos for each of the nine bands and each of N snow types are acquired from a database of snow reflectance spectra, stored in the Snow Reflectance LUT.

   b. Snow anisotropic reflectance factors (ARFs) for each of the nine bands, appropriate for the pixel solar/viewing angles, AOT, and snow type, are acquired from the Snow Reflectance LUT.

   c. The expected observed directional reflectance from each snow type in each band is computed from the narrow band albedos and ARFs.

4) Non-snow reflectance is modeled for each moderate resolution pixel by the *Derive Non-Snow Reflectance* process. The process uses the Monthly Non-Snow Reflectance IP and pre-set BRDF models for each of seven non-snow surface types in the Surface Types-Biomes IP *[Y2402]*, obtained from the BRDF (Biomes) LUT, to derive expected direction reflectance from the non-snow surface. Solar/sensor angles and AOT for each pixel are used to apply the BRDF. The following steps are implemented:

   a. Narrow band non-snow albedos for each of the nine moderate resolution bands are acquired from the Monthly Non-Snow Reflectance IP.

   b. Non-snow ARFs for each of the nine bands, appropriate for the pixel solar/viewing angles and non-snow type, are acquired from a Biomes BRDF LUT. The non-snow surface type is acquired from the Surface Type – Biomes IP.

   c. The expected observed non-snow directional reflectance in each band is computed from the non-snow albedo and the ARFs.

5) Observed surface reflectances from nine VIIRS moderate resolution bands are obtained from the VIIRS Surface Reflectance IP *[Y2411]*. Bad pixels are identified from the Moderate Snow Mask, the Moderate Band Weights, and the Surface Reflectance IP Land Quality Flags (LQF). The *Derive*

Snow Fraction and *Select Snow Type and Fraction* processes calculate snow fraction for each good moderate resolution pixel, using the snow fraction algorithm (Section 3.3.3).

a. Multiple endmember spectral mixture analysis is performed for each snow type, producing snow fraction and error for each type. The snow type with the minimum error is selected, and its snow fraction is reported in the EDR. Optionally, the snow type can also be reported in the EDR, though it is not required.

6) Observed surface reflectances from VIIRS imagery resolution bands I1 (Visible), I2 (Near Infrared - NIR), and I3 (Short Wave Infrared - SWIR) are obtained from the VIIRS Surface Reflectance IP *[Y2411]*. Bad pixels are identified from the Imagery Snow Mask, the Imagery Band Weights, and the Surface Reflectance IP Land Quality Flags (LQF). The *Determine Snow Binary Map* process calculates a snow/no snow binary map for each good imagery resolution pixel, using the snow binary map algorithm adapted from MODIS (Section 3.3.2). The following steps are implemented:

a. The snow type for the co-located moderate resolution pixel is obtained from the snow fraction algorithm. If no type is available, a default snow type is selected.

b. Anisotropic snow reflectance factors (ARFs) for each of the three bands, appropriate for the pixel solar/viewing angles, terrain slope, and snow type, are acquired from the Snow reflectance LUT.

c. Non-snow ARFs for each of the three bands, appropriate for the pixel solar/viewing angles, terrain slope, and non-snow type, are acquired from the BRDF (Biomes) LUT. The non-snow surface type is acquired from the Surface Type – Biomes IP.

d. Narrow band albedos for each of the three bands are computed from the observed directional reflectances and the ARFs, using snow fraction = 0.5.

e. NDSI and NDVI are computed from the narrow band albedos

f. The snow binary threshold tests are applied to the NDSI, NDVI, and NIR band albedo.

7) The binary snow/no snow map for each imagery resolution pixel is written to the VIIRS Snow Cover EDR, along with associated pixel quality flags. The snow fraction for each moderate resolution pixel is also written to the EDR, along with associated pixel quality flags and pixel weights. The snow fraction pixel weight is the total of the individual band weights for that pixel, as determined by the *Make Snow Pixel Masks* process *[Y3234]*.

3.2 ALGORITHM INPUT

3.2.1 VIIRS Data

The snow binary map and snow fraction algorithms require the VIIRS data listed in Table 5.

Table 5. VIIRS Data for the VIIRS Snow Cover Algorithms

Input Data	Source of Data	Reference
Instrument Band Quality	VIIRS SDR*	*[Y2479]*
Geodetic Coordinates	VIIRS SDR*	*[Y2479], [Y3258]*
Solar/Sensor Angles	VIIRS SDR*	*[Y2479]*
VIIRS Grid Reference	VIIRS SDR*	*[Y2479]*
Cloud Mask	VIIRS Cloud Mask IP**	*[Y2412]*
Land/Water Mask	VIIRS Cloud Mask IP**	*[Y2412]*
Forest Mask	Forest LUT***	*[Y3234]*
Aerosol Optical Thickness	Aerosol Optical Thickness IP**	*[Y2471], [Y3277]*
Cloud Optical Thickness	Cloud Optical Thickness IP**	*[Y2471], [Y3277]*
Snow Reflectance Spectra	Snow Reflectance LUT***	*[Y3234]*
Snow Anisotropic Reflectance	Snow Reflectance LUT***	*[Y3234]*
Non-Snow Reflectance Spectra	VIIRS Monthly Non-Snow Reflectance IP**	*[Y2479]*
Non-Snow Surface Type	Surface Type-Biomes IP**	*[Y2402]*
Non- Snow Anisotropic Reflectance	BRDF (Biomes) LUT***	*[Y3234]*
Surface Reflectance	VIIRS Surface Reflectance IP**	*[Y2411]*
Snow Quality Parameters	Snow Quality LUT***	*[Y3234]*
Snow Cover Parameters	Snow Cover LUT***	*[Y3234]*

* SDR = Sensor Data Record ** IP = Intermediate Product *** LUT= Look-up Table

Instrument Band Quality

The Build-SDR module will attach instrument quality flags to the input data. Moderate resolution pixels with bad quality for a given band will be assigned zero band weight. A pixel with a bad SDR quality flag for the I1

band will use band M5 as a substitute. A pixel with a bad SDR quality flag for the I2 band will use band M7 as a substitute. A pixel with a bad SDR quality flag for the I3 band will use band M10 as a substitute. A binary snow map quality flag will be attached to pixels that used a substitute moderate resolution band.

Geodetic Coordinates

Pixel geodetic coordinates will be used to report the latitude/longitude coordinate to the EDR. Terrain slope may be used for BRDF correction.

Solar / Sensor Angles

Pixels with solar zenith angle greater than a threshold shall be excluded from further processing. Our current threshold is 85 degrees. Pixels with solar zenith angle between 70 degrees and 85 degrees will be processed, but with a quality flag attached. The final setting of these values will be made as part of the initialization plan, and may depend upon aerosol optical thickness (AOT). Solar/sensor angles may be used to apply a BRDF quality flag, if warranted by pre-launch or post-launch validation (c.f. Sections 3.6.2, 3.6.3).

VIIRS Grid Reference

Each pixel in the granule will be associated with allocation on the external VIIRS grid. This reference is used to obtain the correct information from the Monthly Non-Snow Reflectance IP and the Surface Types-Biomes IP. The grid reference for each pixel will be included in the EDR file, to allow for post-processing (e.g., time composite products and VIIRS/CMIS combined products).

Cloud Mask

The VIIRS cloud mask *[Y2412]* is expected to derive a status of confident clear / probably clear / probably cloudy / confident cloudy for each pixel, building on MODIS cloud mask heritage (Ackerman *et al.*, 1997). Pixels classified as “cloudy” will be excluded from further processing. Pixels classified as “probably cloudy” are also expected to be excluded. This determination must depend on an assessment of the cloud mask performance, particularly over snow surfaces. Pixels classified as “probably clear” will be processed. For these pixels, the pixel weight will be reduced by a factor obtained from the Snow Quality LUT, and a pixel quality flag will be written to the output EDR. Pixels classified as “confident clear” will be processed with no weight reduction. The cloud mask will also flag pixels that are shadowed by clouds. In that case, a cloud shadow weight reduction factor will be assigned to those pixels and a shadow quality flag will be written to the EDR. The cloud mask will also supply thin cirrus, sun glint, and active fire flags, which our algorithm will use to assign pixel weight and pixel quality to the data.

Land/Water Mask

The EDR will be reported for land pixels. Ocean pixels and Inland Water pixels will be excluded from further processing by having their weight set to zero. Coastline pixel weights will be reduced by a factor obtained from the Snow Quality LUT and reported with a quality flag. Information on Land/Ocean/Inland Water/Coastline status will be obtained from the Cloud Mask IP *[Y2412]*, using the best quality land/water map available.

Forest Mask

A forest mask will be obtained from the Forest LUT, which contains a pre-set array of forest grid locations. A forest canopy quality flag will be assigned to those pixels whose VIIRS Grid Reference matches one of the locations.

Aerosol Optical Thickness

Aerosol optical thickness (AOT) is obtained at moderate pixel resolution from the Aerosol Optical Thickness IP. It is used to derive pixel quality and pixel weight, and also to apply BRDF models.

Cloud Optical Thickness

Cloud optical thickness (COT) is obtained at moderate pixel resolution from the Cloud Optical Thickness IP. It is used to derive pixel quality and pixel weight, as a switchable alternative to the Cloud Mask.

Snow Reflectance Spectra

Snow reflectance is variable, with a strong dependence on grain size and level of impurities. Model spectra from the Johns Hopkins University (JHU) lab are used as baseline spectra, but are not sufficient to model the wider variety of snow types found in nature. A reference library of model snow reflectances will be created as part of the initialization activity.. The work of Nolin and Stroeve (2000) on DISORT modeling of snow albedo can serve as a model for this activity. The number and range of model spectra used will be determined by pre-launch validation activity (c.f. Section 5.1).

Snow Anisotropic Reflectance

Snow anisotropic reflectance factors (ARFs) are needed to derive the expected directional reflectance for a given model snow type. Snow ARFs will be pre-computed and stored in the Snow Reflectance LUT. We plan to compute them from radiative transfer (RT) modeling (c.f. Section 3.3).

Non-Snow Reflectance Spectra

Pixel-by-pixel information about non-snow spectral signatures will be acquired from a reference database indicating the surface properties for the relevant month. The database of non-snow reflectance will be available and corrected on the basis of the latest observations. Initially, we expect the database to be derived from MODIS heritage and improved by NPP. As the NPOESS mission progresses, it will be continually updated as a Monthly Non-Snow Reflectance IP. BRDF corrections are desirable for comparing modeled non-snow reflectance to observed directional reflectance.

Non-Snow Surface Type

The surface type of the underlying non-snow surface is used to apply BRDF correction to the non-snow reflectance. The algorithm uses seven non-snow surface types (Grasses and Cereal Crops, Shrubs, Savannas, Broadleaf Forests, Needleleaf Forests, Broadleaf Crops, and Bare Soil), obtained from the Surface Types-

Biomes IP. Each pixel will be assigned a non-snow surface type by mapping its VIIRS Grid Reference to the IP location.

Non-Snow Anisotropic Reflectance

Anisotropic reflectance factors (ARFs) are needed to derive the expected directional reflectance for a given non-snow surface type. ARFs for seven VIIRS Biomes surface types (Grasses and Cereal Crops, Shrubs, Savannas, Broadleaf Forests, Needleleaf Forests, Broadleaf Crops, and Bare Soil) will be pre-computed and stored in a look up table. The ARF corresponding to the surface type assigned to a given pixel will be used to derive expected directional non-snow reflectance for that pixel.

Surface Reflectance

The VIIRS Surface Reflectance IP [*Y2411*] will provide surface reflectance for all bands used by the algorithms, from atmospheric correction of observed TOA radiance. Models of surface reflectance error are used in our error analysis (c.f. Section 3.4.2).

Snow Quality Parameters

A set of input parameters will be obtained from a pre-set VIIRS Snow Quality LUT. The parameters include a switch determining whether to use the Cloud Mask IP or the Cloud Optical Thickness IP for cloud masking, default relative weights for the nine moderate resolution bands, and weight reduction factors for various types of clouds, AOT, and solar zenith angle (SZA). The values of these parameters will be determined by initialization and validation activities (Section 3.6). A detailed description of the parameters can be found in *[Y3234]*.

Snow Cover Parameters

A set of input parameters will be obtained from a pre-set VIIRS Snow Cover LUT. These parameters direct the implementation of the algorithm (Section 3.3.2). They include I1 and I2 reflectance thresholds, NDSI thresholds, and coefficients used to determine the allowed range of NDVI for a given value of NDSI (c.f. Figures 7 and 8). The values of these parameters have been initialized from MODIS experience (Klein, Hall, and Riggs (1998)) and will be tuned by validation activities (Section 3.6). A detailed description of the parameters can be found in *[Y3234]*.

3.2.2 Non-VIIRS Data

The algorithms use no auxiliary or ancillary non-VIIRS data.

3.3 THEORETICAL DESCRIPTION OF THE RETRIEVAL

The processes outlined in Section 3.1 only apply to regions that have successfully passed the quality examinations. Descriptions of the mathematical backgrounds of these processes follow.

3.3.1 Physics of the Problem

Pure snow is a distinctive target across a part of the solar spectrum. It is among the brightest of natural substances in the visible and near-infrared part of the spectrum, but it is also often the darkest in the shortwave infrared (Dozier, 1989). The spectral albedo of snow depends on wavelength, and this dependency is controlled by the imaginary part *(k)* of the complex refractive index. This reaches a minimum at a wavelength of about 0.46 microns, and increases by a factor of $10^6 – 10^7$ as wavelength increases out to 2.5 microns (Warren, 1982; Dozier, 1989). Light transmission decays exponentially in ice across a distance (d) as $\exp(-4\pi kd/\lambda)$. The *e*-folding distance for ice (the distance over which transmittance is reduced to 1/e) decreases from more than 20 m in the 0.4 – 0.5 micron range to less than 1 mm at 1.6 microns.

Light in snow is scattered primarily by refraction through, not reflection from, the ice grains. Photons are scattered at the grain surfaces, but absorbed while traversing the grain interiors. Only about 3 percent of the light scattered by an ice grain is reflected from the external surface. Nearly 89 percent is refracted through the grain, and 8 percent is scattered after internal reflections (Bohren and Barkstrom, 1974). Because ice is so transparent to visible radiation, snow reflectance is insensitive to grain size in bands below 0.7 microns, but sensitive to absorbing impurities in the snow and to snow water equivalent (SWE; Wiscombe and Warren, 1980; Grenfell, Perovich, and Ogren, 1981). Because absorption by ice is much stronger in bands above 1.4 microns, reflectance at these wavelengths is insensitive to absorbing impurities and SWE, but sensitive to grain size. Absorbing particulates affect snow reflectance out to 0.9 microns (Warren and Wiscombe, 1980), so the 0.86 micron band is sensitive to both absorbing impurities and grain size. All aforementioned values in this paragraph are determined from geometric optics for a sphere.

The spectral signature of snow is unique among common substances. Clouds and snow are both bright across the visible and near-infrared region, but clouds are much brighter than snow in the shortwave infrared. This is because the smaller size of the scatterers in clouds decreases the probability of absorption in this spectral region where ice and water are moderately absorptive (Crane and Anderson, 1984; Dozier, 1984, 1989). Conversely, bodies of open water are dark at all wavelengths. Vegetation is dark in the visible bands because of absorption by photosynthetic pigments, but has a maximum reflectance between 0.7 and 1.3 microns. Because of leaf cell structure (Hoffer, 1978), shortwave infrared reflectance is inversely related to leaf water content for healthy vegetation. Nevertheless, the reflectance at wavelengthslonger than 1.5 microns is still high compared to that of snow. Most rock and soil spectra are the reverse of snow’s. Absorption by iron oxides and organic matter strongly reduce visible reflectances, while those in the shortwave infrared remain high.

Typical reflectance properties of snow and other surfaces are illustrated in Figure 5. An illustration of snow/cloud reflectance differences is in Figure 6.

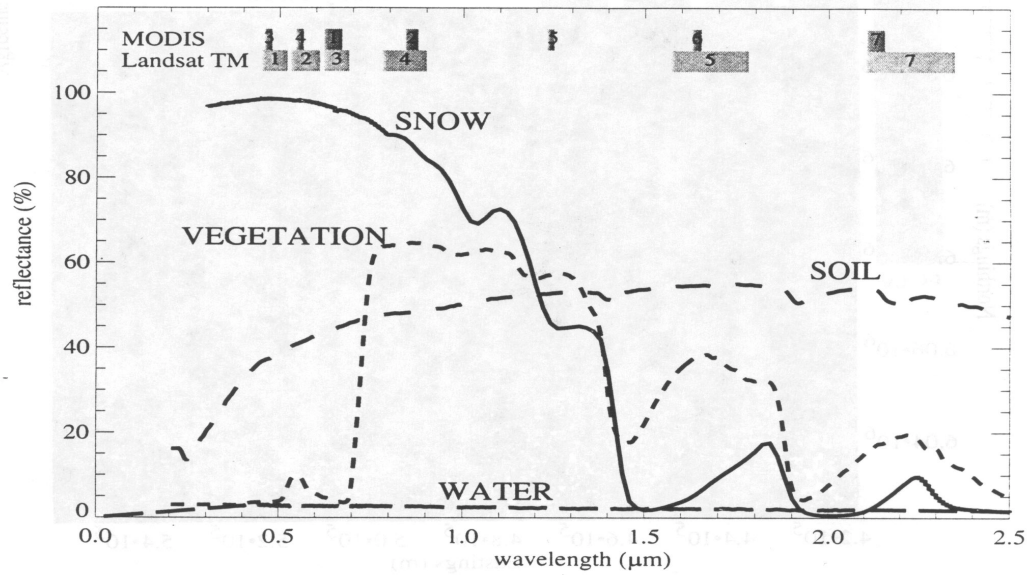

Figure 5: Representative reflectance spectra for snow, vegetation, soil, and water (from Klein, Hall, and Riggs, 1998).

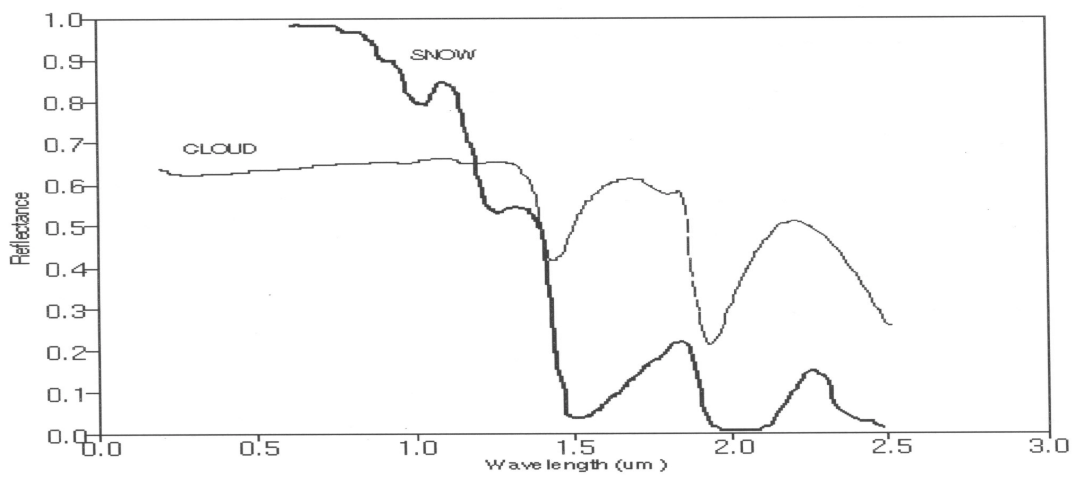

Figure 6: Representative reflectance spectra for snow and clouds (from Hall et al., 1998).

It is important to note that the reflectance spectra shown in the previous figures are representative of one specific case of snow type and cloud type. Real surfaces will exhibit spectral variability for any given surface type. In particular, snow reflectance depends on grain size and impurities. Cloud reflectance will vary with optical thickness, effective particle size, and phase.

The VIIRS Snow Cover EDR requirements apply to snow cover of any depth. Snow is such an efficient scatterer of visible and infrared radiation that the surface reflectance properties of snow are not very sensitive to snow depth or SWE. The physical basis for retrieval of snow depth or SWE is that the scattering efficiency of snow is measurably dependent on frequency in the passive microwave range of the spectrum. Microwave radiation upwelling from the underlying surface is scattered away from the sensor as it propagates through the snowpack. Thus, brightness temperatures at any given microwave frequency are lower for deeper snowpacks. In addition, the scattering efficiency increases with frequency over the microwave range. As a result, differences in brightness temperatures at different microwave frequencies are correlated with the SWE. This physical principle is the basis for SWE retrieval algorithms based on passive microwave observations (Grody and Basist, 1996; Foster, Chang, and Hall, 1997; Chang, 1998).

3.3.2 Mathematical Description of the Snow Binary Map Algorithm

The algorithm is an adaptation of the binary classification technique of the MODIS algorithm, SNOMAP (Hall *et al.*, 1998). SNOMAP classifies snow by a Normalized Difference Snow Index (NDSI) of 0.555 µm and 1.64 µm bands. Our algorithm is an adaptation of the MODIS algorithm. We use an NDSI from the 0.645 µm and 1.61 µm VIIRS imagery resolution bands, combined with a reflectance threshold in the 0.865 µm VIIRS imagery resolution band, to classify a VIIRS pixel as snow or non-snow at imagery resolution.

$$NDSI = (R_1 - R_2) / (R_1 + R_2)$$

Where: R_1, R_2 = Narrow band albedos in 0.645 µm, 1.61 µm MODIS bands

Pixels with an NDSI > 0.4 and a 0.865 µm narrow band albedo > 0.11 are classified as snow. These thresholds have been developed from pre-launch MODIS characterization, as described in the MODIS ATBD (Hall *et al.*, 1998). An illustration of the application of these thresholds is shown as Figure 7.

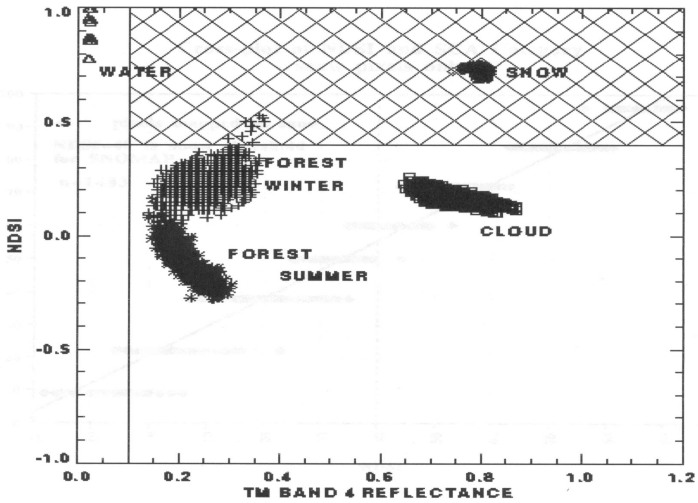

Figure 7: Near-Infrared Reflectance versus NDSI plot for winter and summer Landsat TM scenes of Glacier National Park, Montana (from Hall et al., 1998). Pixels located in the cross-hatched region are classified as snow. Winter forest pixels, which are known to have snow cover under the forest canopy, are incorrectly classified as no snow.

While the NDSI can separate snow from most obscuring clouds, it does not always identify or discriminate optically-thin cirrus clouds from snow. We will follow the MODIS approach (Hall et al., 2001a) by using a thin cirrus mask, derived from reflectance in band M9 (1.37 µm).

The MODIS algorithm also uses a Normalized Difference Vegetation Index (NDVI) to classify snow covered forest pixels by location in an NDSI/NDVI scatter plot.

$$NDVI = (R_1 - R_2) / (R_1 + R_2)$$

Where: R_1, R_2 = Narrow band albedos in 0.858 µm, 0.645 µm MODIS bands

Pixels with 0.1 < NDSI < 0.4 are classified as snow cover under a forest canopy, if NDVI is greater than a threshold value. The threshold depends on the pixel NDSI. These thresholds have been developed from pre-launch MODIS characterization. A snow reflectance model was used in conjunction with a canopy reflectance model (GeoSAIL) to develop the thresholds, which were then tested on Landsat TM images of the southern BOREAS study area in Prince Albert National Park, Saskatchewan. Details can be found in Klein, Hall, and Riggs (1998). An illustration of the application of these thresholds is shown as Figure 8.

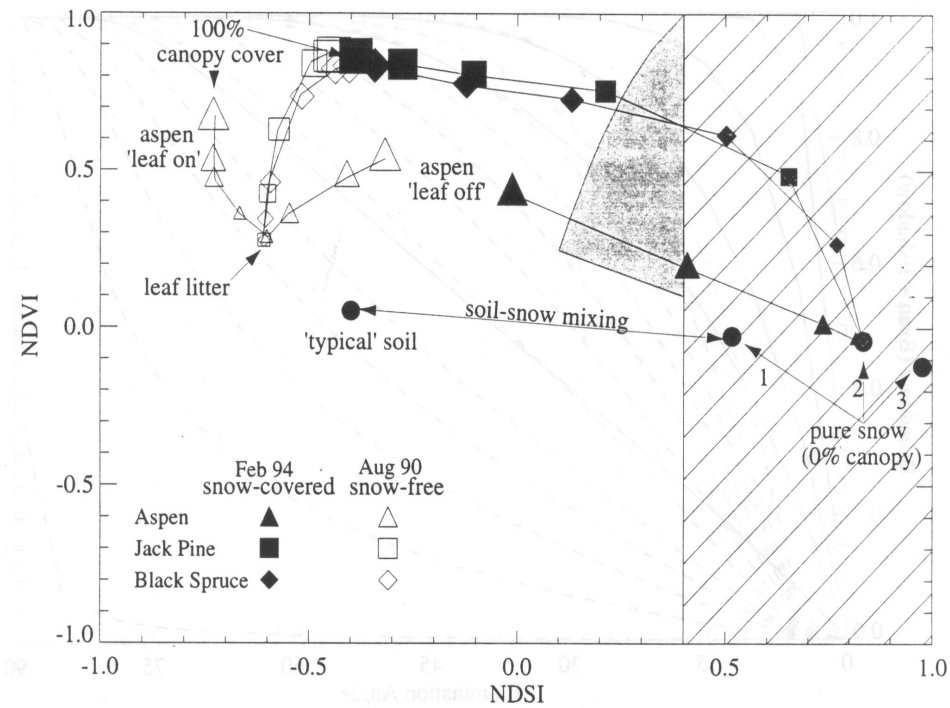

Figure 8: NDSI versus NDVI plot for modeled aspen, jack pine, and spruce stands (from Klein, Hall, and Riggs, 1998). The hatched region is the snow classification region for the Version 4 MODIS algorithm. The gray shaded region represents a proposed additional region for capturing snow-covered forests.

Our algorithm also adopts this approach.

One of the problems facing the MODIS snow-mapping algorithm is the mapping of snow in regions where it is known not to exist. One of the more common locations for this problem is in dark, dense forests, particularly in the tropics. The nature of the snow-mapping algorithm is such that it is particularly sensitive to small changes in the NDSI or NDVI over dark, dense vegetation.

To correct false-snow mappings in tropical forests, the 11.03 µm thermal-infrared band (MODIS band 31) is used to estimate the surface temperature. This band was selected because it represents an atmospheric window, in which little of the emitted thermal radiation is absorbed by the atmosphere. A tentative threshold of 277 K has been set. When this threshold is applied in tropical regions, e.g., the Congo, it eliminates from 93% to 98% of the false snow (Barton, Hall, and Riggs 2001). Our current algorithm does not include this mask, as it has been a very recent MODIS development. We plan to introduce the thermal mask into our algorithm, using the VIIRS M15 band (10.76 µm) brightness temperature as the equivalent to MODIS band 31.

The accuracy of the MODIS snow maps varies with land-cover type (Hall et al., 2001a). This is not surprising, since a single NDSI threshold is applied to surfaces with a variety of characteristic NDSI values. Our algorithm will have the benefit of access to a global surface type database (the VIIRS Surface Type-Biomes IP *[Y2402]*). We can therefore apply surface-type dependent NDSI thresholds, with the potential of improving performance.

3.3.2.1 Correction for Directional Reflectance

The Surface Reflectance IP contains directional surface reflectance. To match the observed directional reflectance to modeled reflectance, we incorporate a directional reflectance correction into our algorithm.

We accomplish the correction with the use of anisotropic reflectance factors (ARFs). The ARF is defined (Nolin and Liang, 2000) as the ratio of the bi-directional reflectance function (BRF) to the narrow band albedo.

$$ARF = BRF(\theta_S, \theta_V, \phi) / \text{Narrow-Band Albedo}$$

Which we write as:

$$\beta(b, \theta_S, \theta_V, \phi) = BRF(b, \theta_S, \theta_V, \phi) / \alpha(b) \qquad (3.3.2.1.1)$$

where:

b = VIIRS band

θ_S = solar zenith angle

θ_v = viewing angle

ϕ = solar-viewing relative azimuth angle

Since the narrow-band albedo is the hemispherically averaged BRF, the hemispherically averaged ARF is unity by definition.

The surface reflectance IP algorithm is designed to produce the surface BRF from observed TOA radiances. We therefore compute narrow band albedo from equation 3.3.2.1.1 as:

$$\alpha(b) = BRF(b, \theta_S, \theta_V, \phi) / \beta(b, \theta_S, \theta_V, \phi) = R_b / \beta(b, \theta_S, \theta_V, \phi) \qquad (3.3.2.1.2)$$

and use $\alpha(b)$ instead of R_b to compute the normalized difference indices:

$$NDSI = (\alpha(1) - \alpha(3)) / (\alpha(1) + \alpha(3)) \qquad (3.3.2.1.3)$$

$$NDVI = (\alpha(2) - \alpha(1)) / (\alpha(2) + \alpha(1)) \qquad (3.3.2.1.4)$$

where:

band 1 = Visible (VIS) imagery resolution band (I1)

band 2 = Near Infrared (NIR) imagery resolution band (I2)

band 3 = Short Wave Infrared (SWIR) imagery resolution band (I3)

Albedos and ARFs for each of the snow types must be pre-computed and stored in LUTs. Nolin and Stroeve (2000) are currently producing these from radiative transfer (DISORT) models for MODIS validation purposes. Given the similarity between the MODIS bands and the VIIRS bands, it is expected that VIIRS LUTs can be constructed in a similar manner.

Non-snow albedos are designed to be available from the VIIRS gridded non-snow reflectance IP. Non-snow type ARFs must be pre-computed and stored in LUTs.

Before applying the threshold tests, we must select a surface type, since the correction factors depend upon surface type. We acquire the snow type from the snow fraction algorithm (Section 3.3.3). If the snow fraction is not available, we select a default snow type. We acquire the non-snow type from the Surface Type – Biomes IP. We compute $\alpha(b)$ for both snow and non-snow cases:

$$\alpha(b\text{: snow}) = R_b / \beta\,(b, \theta_S, \theta_V, \phi : \text{snow}) \qquad (3.3.2.1.5)$$

$$\alpha(b\text{: non-snow}) = R_b / \beta\,(b, \theta_S, \theta_V, \phi : \text{non_snow}) \qquad (3.3.2.1.6)$$

and use narrow band albedo for the case of snow fraction = 0.5:

$$\alpha(b) = 0.5 * (\alpha(b\text{: snow}) + \alpha(b\text{: non-snow})) \qquad (3.3.2.1.7)$$

We use the 0.5 snow fraction case, since the narrow-band albedo thresholds have been developed to classify a pixel as snow when $f > 0.5$ and as non-snow when $f < 0.5$.

MODIS validation has shown a weak relationship between scan angle and the presence of false snow, with more false snow mapped at higher scan angles (Hall et al., 2001a). Numerical tests show that from 35% to 60% of the snow in a given scene can be found at scan angles greater than 45°. It is also observed in the data that almost all of the false snow is mapped on the sunward side of the sensor. This phenomenon is probably due to forward scattering off of various atmospheric or ground-level agents. It is expected that BRDF correction of VIIRS reflectance will mitigate most of this effect. VIIRS validation (Section 4.5) will test this expectation. In the event that significant forward scattering error still exists, a quality flag will be set for all affected scan angles.

3.3.3 Mathematical Description of the Snow Fraction Algorithm

The hypothesis that snow fraction can be determined by assuming that observed reflectance spectra are linear combinations of the spectra of a small set of scene components (spectral endmembers) has been supported by several studies (Nolin, Dozier, and Mertes, 1993; Rosenthal, 1993; Rosenthal and Dozier, 1996). These endmembers are the spectra of snow, rock, soil, or vegetation. They can be obtained from the image itself (image endmembers), or from calibrated field or laboratory spectra (reference endmembers). The algorithm to retrieve snow fraction includes an application of linear spectral unmixing. Spectral mixture analysis “unmixes”

the mixed pixels determining the fraction of each spectral endmember that would combine to produce the mixed pixel's spectral signature.

Our approach is based on a mixture model which incorporates multiple snow endmembers to characterize subpixel snow cover. The technique is called Multiple Endmember Spectral Mixture Analysis (MESMA). Snow's spectral reflectance is sensitive to grain size, impurity, water content and other attributes. As a result, snow spectrally manifests itself as a range of endmembers. Thus, multiple snow endmembers are desirable to increase the accuracy of the snow cover retrieval. Use of multiple snow endmembers improves spectral mixture analysis. This approach is based on translation of varying snow parameters into different snow spectral reflectance. The variable spectral nature of snow is accounted for by use of multiple snow endmembers (Painter et al., 1998).

Significant sub-scene heterogeneity can contaminate spectral mixture analysis (SMA) modeling with a fixed suite of endmembers. To increase the accuracy of the algorithm, we assume variation of the endmembers on a pixel-by-pixel basis. The algorithm takes into account the most prominent features of the endmember spectra varying from one location on the earth surface to another. We use MESMA allowing the endmembers to vary on a pixel-by-pixel basis, which accounts for variation in surface types both for snow and non-snow endmembers. Such an approach has been developed by Painter et al. (1998) and Roberts et al. (1998). It has been shown in these papers that reference endmember libraries can be used with great success to accurately map snow in alpine regions and in the Santa Monica Mountains.

Our approach is based on using a mixture model with known non-snow endmembers for each pixel. The snow cover (fraction) for the pixels is estimated by the mixture model with least mixing mean-square-root error. Our approach allows the types of snow endmembers to vary on a per pixel basis. It is assumed that the true reflectance is a linear combination of the non-snow reflectance and a single snow type reflectance:

$$M_{bt} = f\ S_{bt} + (1-f)\ X_b \qquad (3.3.3.1)$$

where: f = True snow fraction.

M_{bt} = Model reflectance in band (b) for snow type (t) and snow fraction (f).

S_{bt} = Model reflectance in band (b) for snow type (t).

X_b = Model non-snow reflectance in band (b).

The root mean square (RMS) variance of the observed reflectance from the model reflectance is:

$$e_t^2 = \Sigma\ (R_b - f\,(S_{bt} - X_b) - X_b)^2\ w_b \qquad (t = 1,N) \qquad (3.3.3.2)$$

where: R_b = Observed reflectance in band (b).

w_b = Weight in band (b).

and the summation is over all bands.

Minimization of e_t^2 with respect to f_t gives us the snow fraction for snow type (t):

$$f_t = \Sigma \; (R_b - X_b)(S_{bt} - X_b)\, w_b \; / \; \Sigma \; (S_{bt} - X_b)^2 \; w_b \qquad (3.3.3.3)$$

where the summations are over all bands.

For each of the N snow types, the algorithm computes f_t from equation (3.3.3.3). Fractions smaller than zero are set to zero. Fractions greater than one are set to one. The algorithm then computes e_t^2 by plugging f_t back into equation (3.3.3.2). The type (t) with the smallest e_t^2 is selected, and its f_t is reported as the snow fraction.

3.3.3.1 Correction for Directional Reflectance

The Surface Reflectance IP contains directional surface reflectance. To match the observed directional reflectance to modeled reflectance, we incorporate a directional reflectance correction into our algorithm.

We accomplish the correction with the use of anisotropic reflectance factors (ARFs). The ARF is defined as the ratio of the bi-directional reflectance function (BRF) to the narrow band albedo.

We treat the observed reflectance as the product of a narrow band albedo and a directional correction factor. In that case, we write the snow and non-snow reflectances as:

$$S_{bt} = \alpha_{bt} \; \beta_{bt} \qquad (3.3.3.1.1)$$

$$X_b = \alpha_{Bx} \; \beta_{Bx} \qquad (3.3.3.1.2)$$

where: α_{bt} = Band (b) albedo for snow type (t) (hemispherically averaged BRF)

$\beta_{bt} = \beta_{bt}(\theta_S(p), \theta_V(p), \phi(p))$ = ARF for pixel (p), band (b), and snow type (t)

α_{Bx} = Band (b) albedo for non-snow type (X) (hemispherically averaged BRF)

$\beta_{Bx} = \beta_{Bx}(\theta_S(p), \theta_V(p), \phi(p))$ = ARF for pixel (p), band (b), and non-snow type (X(p))

and use the directionally corrected S_{bt} and X_b in equations 3.3.3.2 and 3.3.3.3.

Snow albedos and correction factors must be pre-computed and stored in LUTs. Nolin and Stroeve (2000) are currently producing these from radiative transfer (DISORT) models for MODIS validation purposes. Given the similarity between the MODIS bands and the VIIRS bands, it is expected that VIIRS LUTs can be constructed in a similar manner.

Non-snow albedos are designed to be available from the VIIRS gridded non-snow reflectance IP. Non-snow type ARFs must be pre-computed and stored in LUTs.

3.3.3.2 Endmember Selection (Non-Snow Reflectance)

The construction of Equation 3.3.3.1 requires us to select the endmembers that constitute a given pixel in a scene. This is perhaps the largest constraint on the use of spectral unmixing as an operational approach to subpixel snow mapping.

Previous results of using MESMA (Roberts et al., 1998) show that a majority of the image could be modeled as two-endmember models. Three-endmember models provide poorer discrimination due to overlap of different models. Therefore, we limit our choice to two endmembers (one for snow and one for the non-snow background). In general, the lower the number of endmembers, the higher the priority in choosing endmembers for SMA. But using MESMA along with the database of non-snow endmembers allows us to avoid constraints related to application of 2 endmembers.

The regional nature of endmembers presents the greatest hindrance for development of the algorithm. Our approach treats the non-snow endmember as an empirical quantity derived from observations, rather than a pure surface type.

Our proposed approach eliminates the search for endmembers on the fly, which significantly increases the speed of calculations, making possible operational usage. Optimal speed and efficiency are achieved when the information on non-snow endmember reflectance is available and accurate. Features of non-snow endmembers change from pixel to pixel. The reflectance spectral signatures of non-snow endmembers are a source of error, since the conditions of the underlying surface at a particular location will vary seasonally.

MESMA has been successful in regional mapping of snow fraction. Given this success, there is good reason to expect the technique can be developed so that it is operational on a global basis. There is some risk associated with applying the algorithm globally, since the required global database of non-snow reflectance does not currently exist.

We plan to build a global library of monthly mean non-snow reflectance in the VIIRS bands to account for seasonal variations. The library will be built from satellite observations rectified to a fixed latitude/longitude grid. MODIS will produce a surface reflectance product (Vermote, 1999), which will be used to build an initial database. The MODIS bands are similar to the VIIRS bands. Rectification of the MODIS data to the VIIRS bands should therefore introduce minimal error. Observations during the NPP will build on the MODIS database and customize it to the VIIRS bands.

3.3.3.3 Snow Reflectance

The reflectance spectral signatures of snow endmembers will be obtained from a reference database, which we will build. There are different ways to collect information on snow spectral signatures. These include analytic derivations from scattering theory, observations under laboratory conditions, *in situ* observations, and remote observations from orbiting satellites.

3.3.3.4 Atmosphere / BRDF Coupling

A rigorous approach to obtaining narrow-band albedo from observed TOA radiance would couple the atmospheric (aerosol) and surface reflectance effects. Our approach does not couple the effects. We use a directional surface reflectance IP produced by an atmospheric correction that accounts only for the coupling effects of BRDF, and then apply an anisotropic reflectance correction. We expect our approach to be sufficiently accurate to meet the EDR specification *[Y2411]*. EDR performance analysis with MODIS Terra, MODIS Aqua, and VIIRS NPP data will provide verification of our approach.

3.3.4 Archived Algorithm Output

Algorithm output will be written to the VIIRS Snow Cover EDR, in HDF EOS format. The binary snow map will be archived at imagery pixel resolution as a yes/no bit for each pixel, along with associated pixel quality flags. The retrieved fraction of snow for each VIIRS pixel will be archived at moderate pixel resolution, along with associated pixel quality flags and snow fraction pixel weights.

3.3.5 Algorithm Watch List

Following its review of the Version 3 ATBDs, the VIIRS Operational Algorithm Team (VOAT) has produced a list of items requiring attention. Three of these, items 5, 7, and 8, directly affect the Snow EDR:

> 5) *SURFACE DIRECTIONAL EFFECTS – "Consideration of surface directional effects will better address EDRs (Albedo, VI, Snow Cover) based on solar reflective bands. There is insufficient use of BRDF-modeled surfaces in Phase I analyses for land EDRs, angle-dependent surface reflectance/VI products and insufficient documentation of intermediate products."*
>
> *6) SNOW COVER – "Snow Cover EDR performance at large solar zenith angles and for various cloud cover and surface conditions. Possible disadvantage is dependence on absolute reflectance. Atmospheric correction errors should be studied in detail and BRDF effects. MODIS derived non-snow spectra will be very limited by discrete MODIS sun-view geometries."*
>
> *8) IMPACT OF CLOUD MASK – "Impact of Cloud Mask (clear, cloudy, aerosol distinction) for EDR production and performance."*

3.3.5.1 Surface Directional Effects

5) *"Consideration of surface directional effects will better address EDRs (Albedo, VI, Snow Cover) based on solar reflective bands. There is insufficient use of BRDF-modeled surfaces in Phase I analyses for land EDRs, angle-dependent surface reflectance/VI products and insufficient documentation of intermediate products."*

In our response, Raytheon stated that a "BRDF-correction solution is being developed for V4 of the Snow Cover ATBD (this document)." Accordingly, the VOAT cancelled this item for snow. Our BRDF-correction approach is discussed in Sections 3.3.2.1 and 3.3.3.1 of this document.

3.3.5.2 Snow Cover

"Snow Cover EDR performance at large solar zenith angles and for various cloud cover and surface conditions. Possible disadvantage is dependence on absolute reflectance. Atmospheric correction errors should be studied in detail and BRDF effects. MODIS derived non-snow spectra will be very limited by discrete MODIS sun-view geometries."

In our response, we stated that "Raytheon concurs that the solar zenith angle over snow will often exceed current solar zenith angle limits of 70 degrees on specification performance for the Snow Cover EDR. Phase I solutions stipulated that beyond limits, the EDR would be reported but not guaranteed to meet the specification, as indicated in the Algorithm Subsystem Specification. This will be clarified in versions four and five of the Snow Cover ATBD, as well as for all other ATBDs where the issue currently is not clarified. The development of the monthly non-snow reflectance IP will begin in Phase II by using MODIS data."

We recognize that effective cloud masking is essential to the production of an operational fresh water ice product from Vis-IR data. We are sensitive to the concern in the user community that very aggressive cloud masking can result in the unnecessary exclusion of useful surface data observable through thin clouds. We have been working with the VIIRS Cloud Integrated Product Team (IPT) to provide a Cloud Mask Intermediate Product that will enable us to process and report the Snow Cover EDR for surfaces observable through thin cloud cover. Our plan is to identify three regions in the "Cloud Optical Thickness" phase space. In the "Green" region (small τ), the EDR will be reported to meet or exceed specification. In the "Red" region (large τ), the pixel will be masked and the EDR will not be reported. We plan to define a "Yellow" transition region, where the EDR will be reported with a quality warning attached. In this region, we expect the algorithm performance to be degraded below specification, but still to provide useful information. Pixels in the "Yellow" region will have their weight reduced by a factor obtained from the Snow Quality LUT. Weight reduction factors will be determined from initialization activity, using MODIS data, and will be refined with NPP/VIIRS data. The cloud optical thickness thresholds that identify the three regions are TBD, and will require validation with MODIS and NPP/VIIRS data.

We also understand that atmospheric correction is particularly challenging over bright surfaces such as snow. Atmospheric correction is performed by the Surface Reflectance algorithm *[Y2411]*, and is outside the scope of the Snow algorithm. Our approach for atmospheric correction over snow/ice surfaces is to use nearby dark pixels for aerosol definition. If there are no nearby dark pixels, we use aerosol climatology as a fall back. Refer to *[Y2411]* for a discussion.

The VOAT has cancelled this item.

3.3.5.3 Impact of Cloud Mask

"Impact of Cloud Mask (clear, cloudy, aerosol distinction) for EDR production and performance."

In our response to the watch list, we stated that "Raytheon agrees that the interplay between the Cloud mask and the rest of the VIIRS system is a central issue leading into CDR. Within the scope of Phase II, Raytheon will further refine the definitions of 'probably cloudy' and 'probably clear'."

We recognize that effective cloud masking is essential to the production of a global operational snow product from Vis-IR data. We have addressed this matter in Section 4.3.1. We will continue to work with the Cloud IPT and the VOAT to ensure that the VIIRS Cloud Mask algorithm provides a product of sufficient quality for us to meet our specification for the Snow EDR.

4.0 EDR PERFORMANCE

The performance of the algorithms with respect to the VIIRS requirements and the System Specification (c.f. Tables 1 and 2) is reviewed in this section.

EDR performance shall be verified by analysis, modeling, and/or simulation based on the instrument design and performance characteristics and the algorithms. The analysis, modeling, and/or simulation shall be sufficiently extensive in scope to verify that EDR requirements are met under a broad range of conditions that are representative of those occurring in nature, include typical and extreme conditions.

4.1 STRATIFICATION

4.1.1. Snow Binary Map

We identify the following stratifications for the snow binary map:

i. Snow fraction “truth”

ii. Sensor view angle

iii. Solar zenith angle

iv. Fraction of mixed pixels

Performance of the snow binary map algorithm will depend on snow fraction. The probability of correct typing for any binary classifier must approach 50% as the threshold for defining yes/no “truth” is approached. Our algorithm thresholds have been tuned to a threshold of 0.5 in snow fraction. That is, the probability of correct typing will increase as true fraction differs from 0.5. A sensible stratification must then include snow fraction “truth” as a parameter. We have selected 5 ranges of snow fraction, 0.0-0.2, 0.2-0.4, 0.4-0.6, 0.6-0.8, and 0.8-1.0. We have deliberately selected these ranges so that they are symmetric with respect to 0.5, where we expect minimum EDR performance.

The requirements are specified at nadir. Our stratification of sensor view angle is restricted to nadir view.

We have used a solar zenith angle of 60 degrees in our simulations to date. Our stratification of solar zenith angle is restricted to this value. A wider range of solar zenith angles shall be simulated in the future, following the development of surface reflectance error simulations over a wider range.

It is informative to report EDR performance for a representative range of structured scenes. We parameterize this range as a stratification by fraction of mixed pixels in a scene. Scenes with a greater fraction of mixed pixels are expected to have a reduced EDR performance because spatial errors (MTF, band misregistration) are greater and because the binary classifier must degrade as snow fraction approaches 0.5. We have selected three stratifications by fraction of mixed pixels, 10% (easy), 30% (typical), and 50% (hard).

4.1.2 Snow Fraction

We identify the following stratifications for the snow fraction:

v. Snow fraction "truth"

vi. Sensor view angle

vii. Solar zenith angle

viii. Fraction of mixed pixels

Performance of the snow fraction algorithm is expected to depend on snow fraction ("truth"). We have selected 4 ranges of snow fraction, 0.0-0.25, 0.25-0.5, 0.5-0.75, and 0.75-1.0.

Unlike the binary snow map, the snow fraction requirements are specified at worst case as well as nadir. Our stratification of sensor view angle includes nadir and edge-of-scan views.

We have used a solar zenith angle of 60 degrees in our simulations to date. Our stratification of solar zenith angle is restricted to this value. A wider range of solar zenith angles shall be simulated in the future, following the development of surface reflectance error simulations over a wider range.

It is informative to report EDR performance for a representative range of structured scenes. We parameterize this range as a stratification by fraction of mixed pixels in a scene. Scenes with a greater fraction of mixed pixels are expected to have a reduced EDR performance because spatial errors (MTF, band misregistration) are greater. We have selected three stratifications by fraction of mixed pixels, 10% (easy), 30% (typical), and 50% (hard).

4.2 STRATIFIED PERFORMANCE ANALYSIS

4.2.1. Snow Binary Map

Performance verification is by demonstration.

We classified MODIS Airborne Simulator (MAS) scenes as snow or no snow at a 50 meter pixel resolution, with the aid of an unsupervised 6 band classification in ENVI. Manual review of the ENVI classifications was performed to assign each ENVI-derived class as snow or no snow.

We aggregated each scene to pixel sizes of 0.4 km and 0.8 km to simulate VIIRS pixels at nadir and edge of scan respectively. We classified each VIIRS pixel as snow or no snow, depending upon the number of snow/no snow MAS pixels in the aggregate. At nadir, a VIIRS pixel is an aggregate of 64 MAS pixels. For a VIIRS nadir pixel to be classified as snow, it required 33 or more MAS pixels classified as snow. For a VIIRS nadir

pixel to be classified as no snow, it required 33 or more MAS pixels classified as no snow. These classifications are used as "VIIRS truth".

A number of perturbations were applied to the scenes to simulate sensor/algorithm performance.

Reflectance errors were applied to the scenes. We perturbed the aggregated reflectances in MAS bands 3 (648 nm), 7 (866 nm), and 10 (1.63 µm), using model errors for the Surface Reflectance IP in VIIRS bands 5i (645 nm), 6i (865 nm), and 8i (1.61 µm). We have obtained these from the performance analysis of the Surface Reflectance algorithm *[Y2411]*. Reflectance accuracy errors were modeled by assuming an aerosol optical thickness (AOT) of 0.1 and a 0.05 offset between true AOT and the AOT acquired from a climatological database. Details on the creation and use of the aerosol climatology are found in the Aerosol Optical Thickness and Particle Size Parameter ATBD *[Y2388]*. Our selection of AOT mean and offset is based on studies of typical aerosol conditions in the sub-arctic (Blanchet and List, 1983). Reflectance precision errors were modeled from the sensor noise performance specification. The reflectance errors depend on surface reflectance truth, which is correlated with snow fraction. Reflectance errors were calculated for a solar zenith angle of 60 degrees.

Spatial errors were also applied to the scene. The scenes were perturbed by MTF smearing, following the sensor MTF performance specification. Band misregistration was simulated by offsetting the NIR and SWIR bands by 0.2 pixels with respect to the visible band, consistent with the VIIRS sensor specification for band registration *[PS154640-101]*.

We applied the algorithm to the perturbed VIIRS scenes to retrieve snow/no snow, and computed probability of correct typing by comparing the retrieved classifications to the "VIIRS truth". We did this for four scenes:

ix. A Death Valley scene containing no snow cover (SUCCESS_115_16)

x. A Brazil scene containing no snow cover (SCAR-B_163_1)

xi. A Northern Minnesota scene containing 100% snow cover under a varying canopy (WINCE_49_06)

xii. A mixed snow/no snow scene in Colorado in February (WINCE_50_14)

The first two scenes test the algorithm performance over desert and vegetated non-snow surfaces. The third scene tests the performance in winter forest regions. The fourth scene tests the performance for a typical case of mixed snow/no snow pixels.

Death Valley Scene: Visible (.645 µm) and SWIR (1.6 µm) images of the scene are shown in Figure 9. There is of course no snow in the scene. The bright feature is a salt pan. It can not be distinguished from snow by the visible data alone (Figure 9a), but its brightness in the SWIR (Figure 9b) does distinguish it from snow.

(a) **(b)**

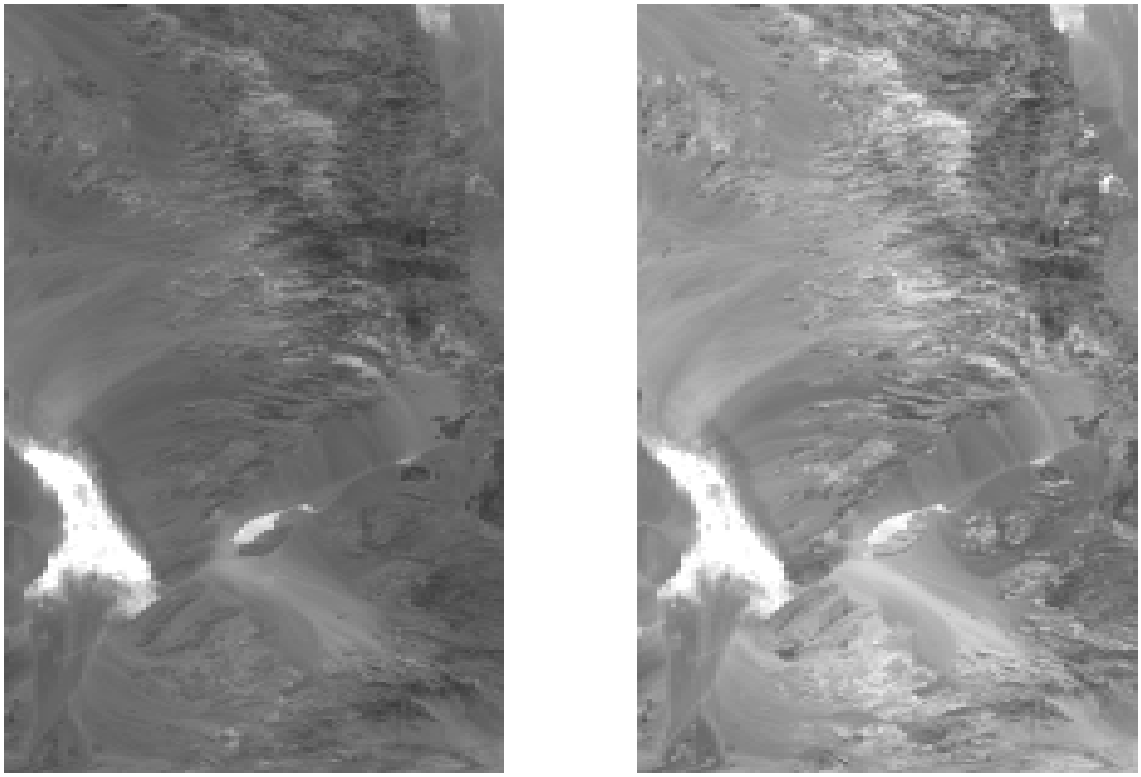

Figure 9: (a) Visible reflectance image of Death Valley scene from MAS/SUCCESS campaign. The grey-scale is from 0.0 to 0.5 in reflectance. (b) Short Wave IR reflectance image of the scene. The grey-scale is from 0.0 to 0.5 in reflectance.

The NDSI/NDVI scatter plot for the Death Valley scene is shown in Figure 10. Expected system performance errors were added to the scenes.

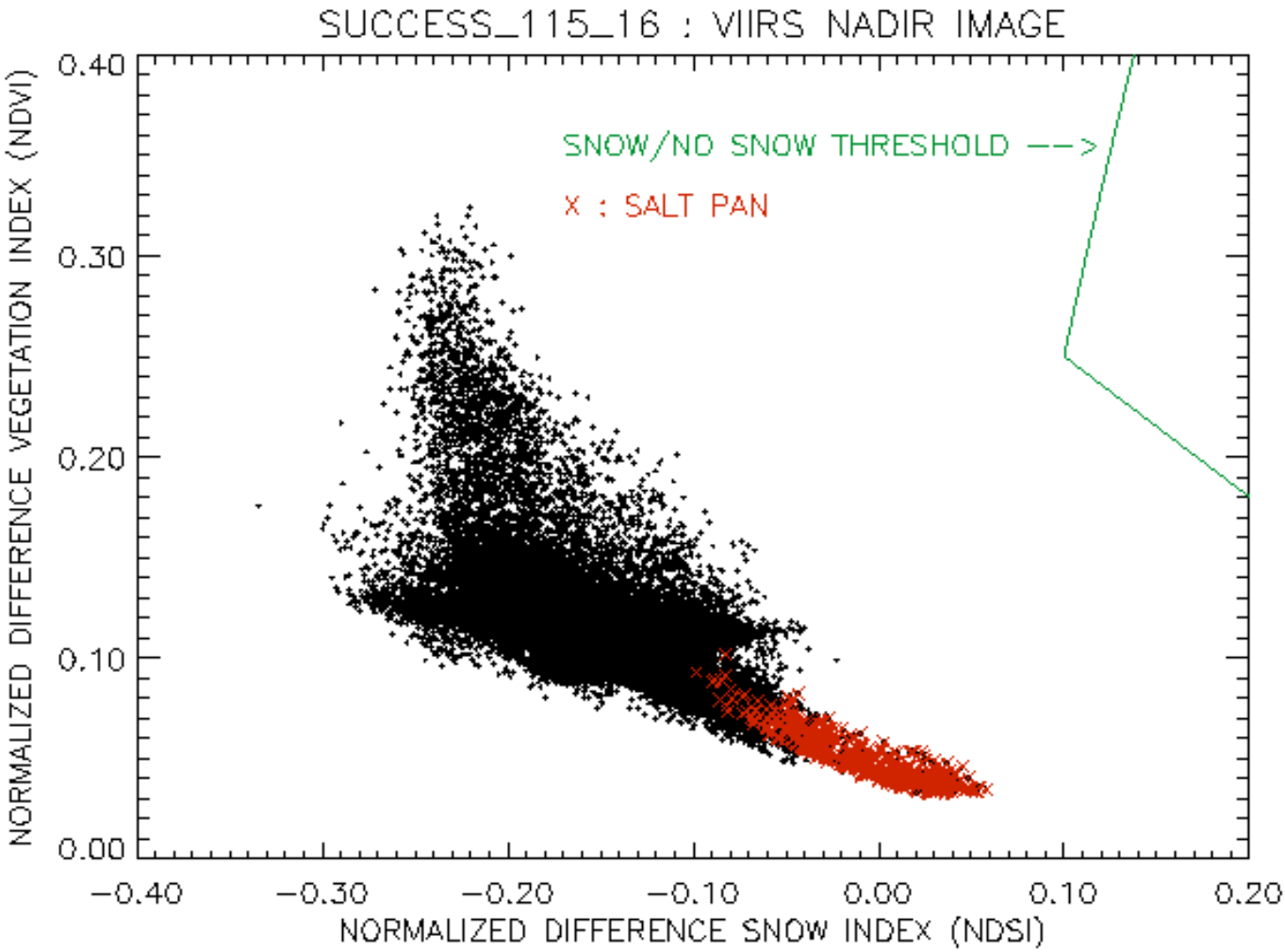

Figure 10: NDSI versus NDVI scatter plot of the MAS Death Valley scene (SUCCESS_115_16). The image has been aggregated to a VIIRS pixel size at nadir.

Correct classification occurs when pixels classified as snow fall to the right of the green threshold boundary and when pixels classified as no snow fall to the left of the boundary. All pixels in this scene were correctly classified as no snow, including the salt pan.

Brazil Scene: Visible (.645 µm) reflectance, NDVI, and NDSI images of the scene are shown in Figure 11. There is of course no snow in the scene.

(a) **(b)** **(c)**

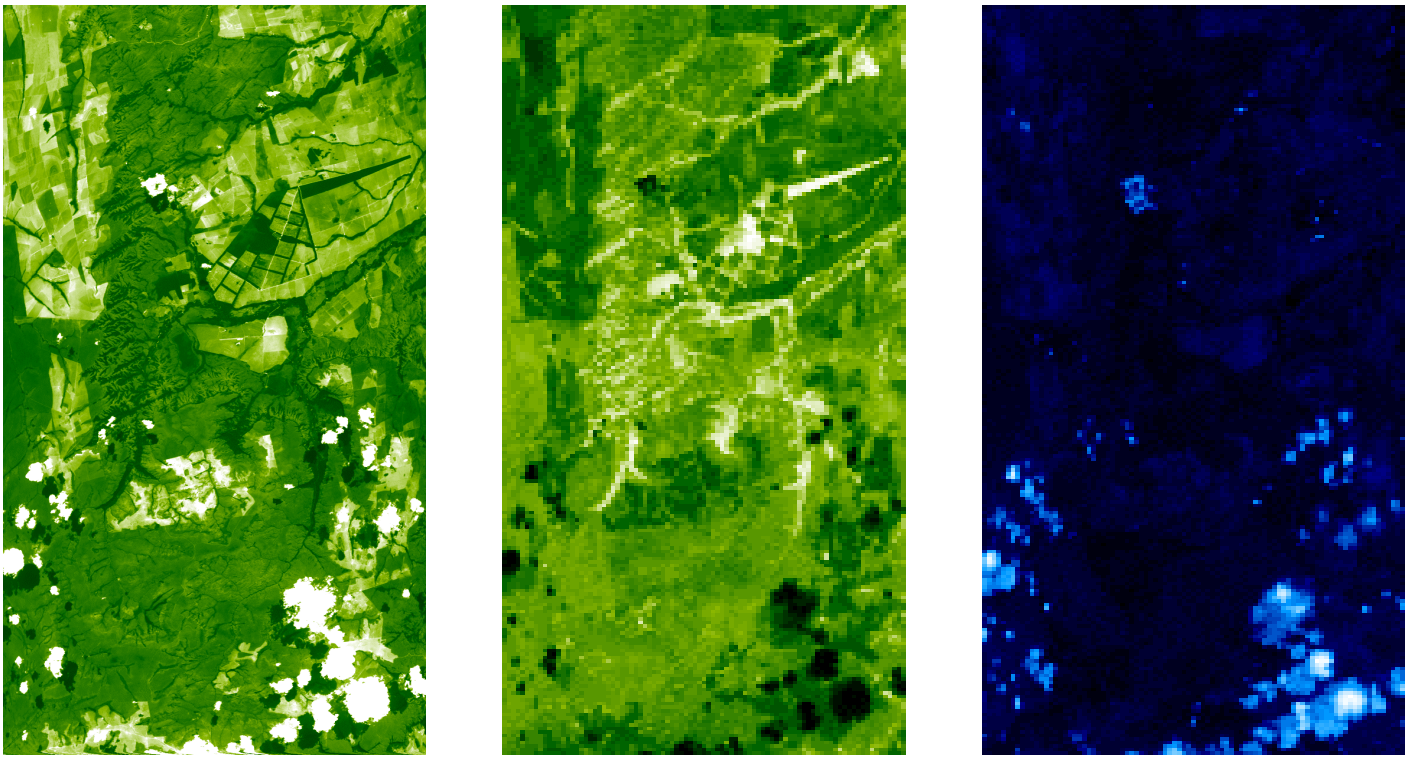

Figure 11: (a) Visible reflectance image of Brazil scene from MAS/SCAR-B campaign. The color scale is from 0.0 to 0.2 in reflectance. (b) NDVI image of the scene. The color scale is from 0.05 to 0.7 in NDVI units. (c) NDSI image of the scene. The color scale is from –0.5 to 0.07 in NDSI units.

The NDSI/NDVI scatter plot for the Brazil scene is shown in Figure 12. Expected system performance errors were added to the scenes.

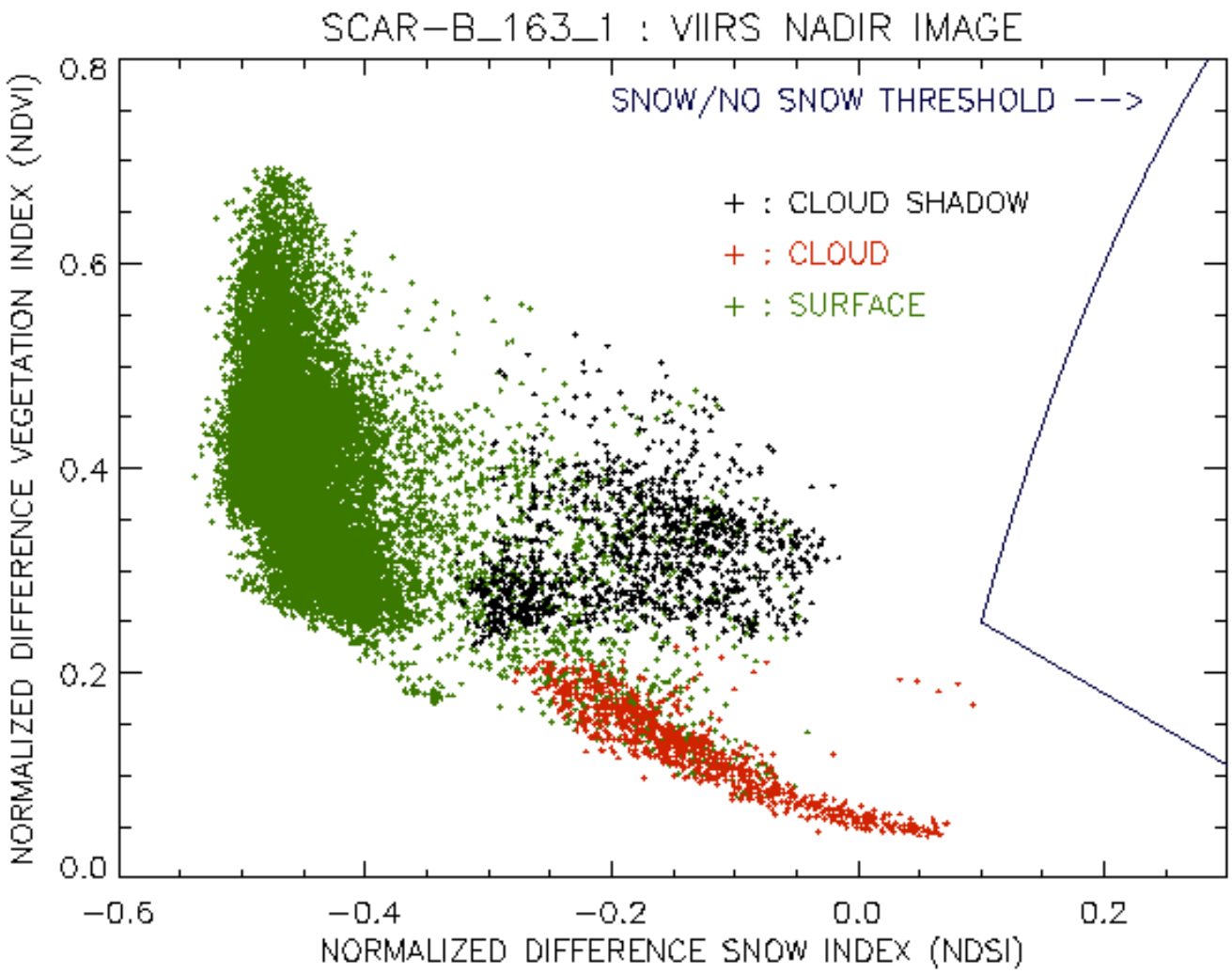

Figure 12: NDSI versus NDVI scatter plot of the MAS Brazil scene (SCAR-B_163_1). The image has been aggregated to a VIIRS pixel size at nadir.

Correct classification occurs when pixels classified as snow fall to the right of the blue threshold boundary and when pixels classified as no snow fall to the left of the boundary. All pixels in this scene were correctly classified as no snow, including the cloud and cloud shadow pixels.

Minnesota Winter Scene: Visible (.645 μm) reflectance is shown in Figure 13a. Manual review of the ENVI-classified scene has established that the scene is 100% snow covered. The large variation in reflectance is caused by a variation in the forest canopy over the snow covered surface. The NDSI image is shown in Figure 13b. Brighter areas have larger NDSI. These areas have a lighter forest canopy. The NDVI image is shown in Figure 13c. Darker areas have larger NDVI. These areas have a denser forest canopy.

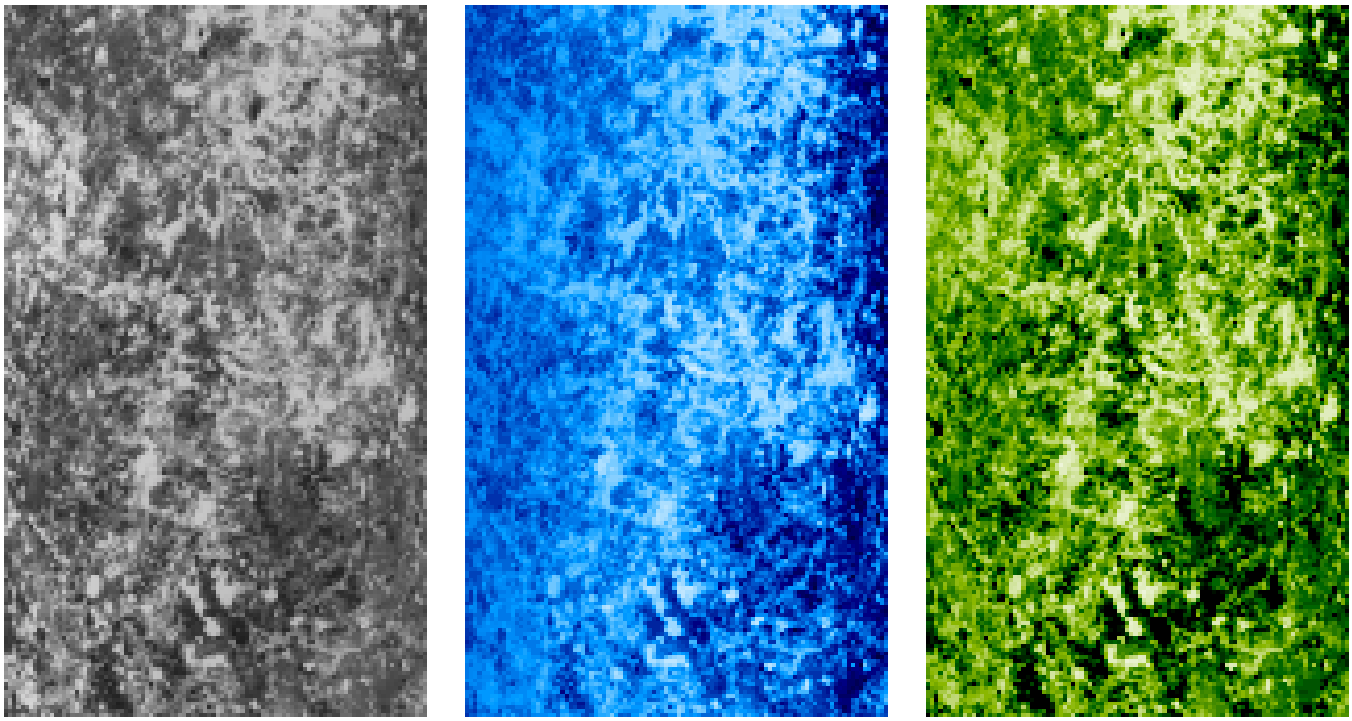

Figure 13: (a)Visible reflectance image of Minnesota winter scene from MAS/WINCE campaign. The grey-scale is from 0.0 to 1.0 in reflectance. (b) Normalized Difference Snow Index (NDSI) image of the scene. The color scale is from NDSI = 0.0 (darkest) to NDSI = 0.8. (c) Normalized Difference Vegetation Index (NDVI) image of the scene. The color scale is reversed, from NDVI = 0.25 (darkest) to NDVI = 0.05.

The NDSI/NDVI scatter plot for the MAS Minnesota winter scene is shown in Figure 14. Expected system performance errors were added to the scene. All of the VIIRS pixels were correctly classified as snow.

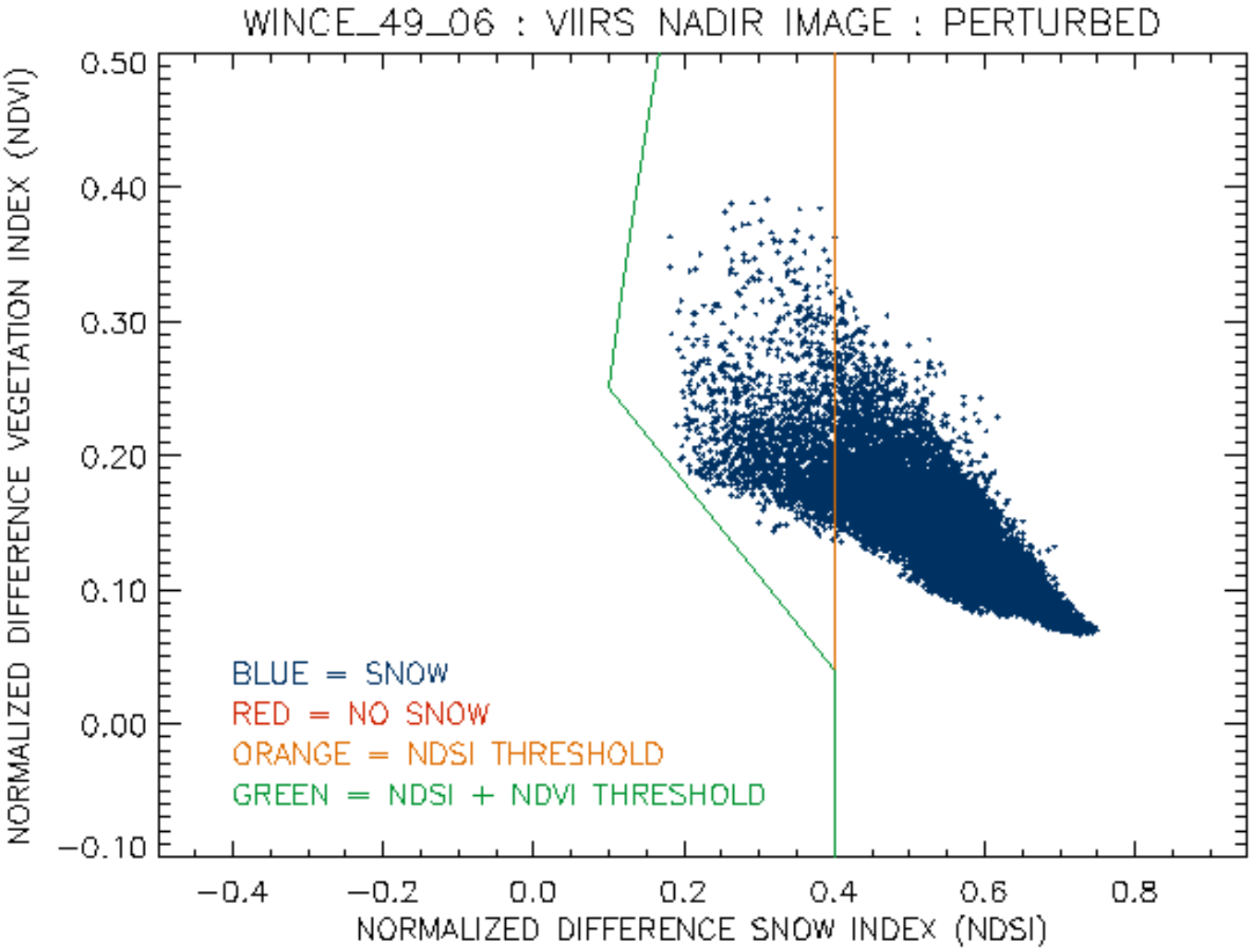

Figure 14: NDSI versus NDVI scatter plot of the MAS Minnesota winter scene (WINCE_49_06). The image has been aggregated to a VIIRS pixel size at nadir.

Comparison of this figure to Figure 13 indicates that the scene can be characterized as a uniform snow-covered surface under a variable forest canopy. As the density of the canopy increases, the location in the scatter plot moves up and to the left, resulting in a canopy-density track. Correct classification occurs when pixels classified as snow (blue) fall to the right of the green threshold boundary and when pixels classified as no snow (red) fall to the left of the boundary. All pixels in this scene are correctly classified as snow. Without the NDVI correction, misclassification would occur where blue pixels fall to the left of the orange boundary, resulting in a correct classification of 91.6 %.

Colorado Winter Scene: Visible (.645 µm) reflectance is shown in Figure 15a. Manual review of the ENVI-classified scene has established that the scene has a mixture of snow cover. Aggregation of the classified pixels to a VIIRS nadir resolution produces a snow fraction "truth" image, shown in Figure 15b. The scene was perturbed by our model for system error, and our binary map algorithm applied to the perturbed data. The result is shown in Figure 15c.

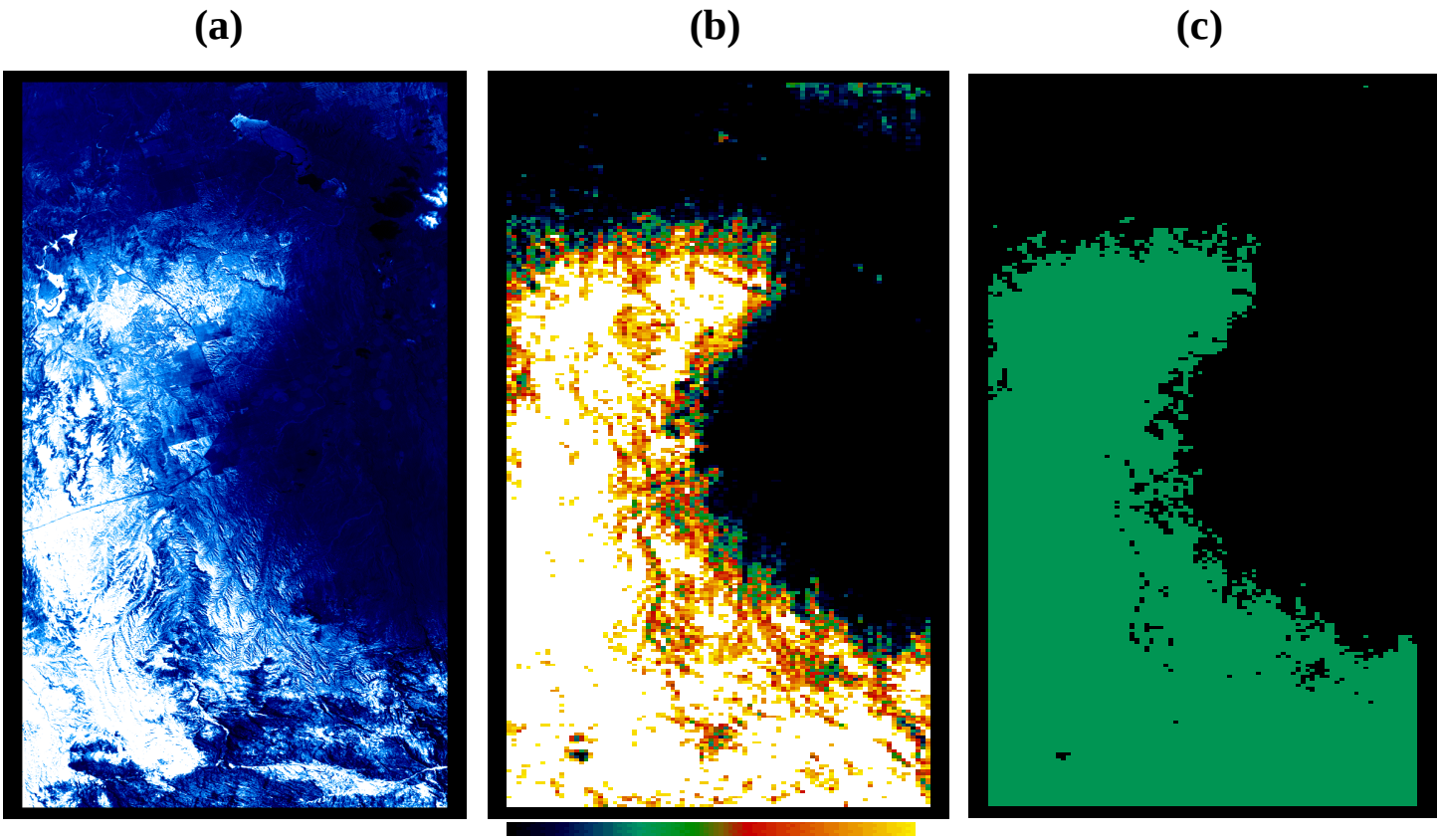

Figure 15 (a) Visible Reflectance at 50 meter resolution, taken from a 0.648 micron image of Eastern Colorado obtained by the MODIS Airborne Simulator (MAS) on February 13, 1997. The extent of the scene is 35 km x 100 km. (b) Snow fraction at 0.4 km resolution, obtained by classification and aggregation to a VIIRS pixel size at nadir. (c) Retrieved Binary Snow Cover map. System performance errors were used to simulate a VIIRS retrieval. Green cells are mapped as snow. 97.8 % of the pixels were correctly typed.

Figure 16 shows an NDSI versus NDVI scatter plot for the Colorado winter scene, aggregated to a VIIRS pixel size at nadir, with no error perturbations.

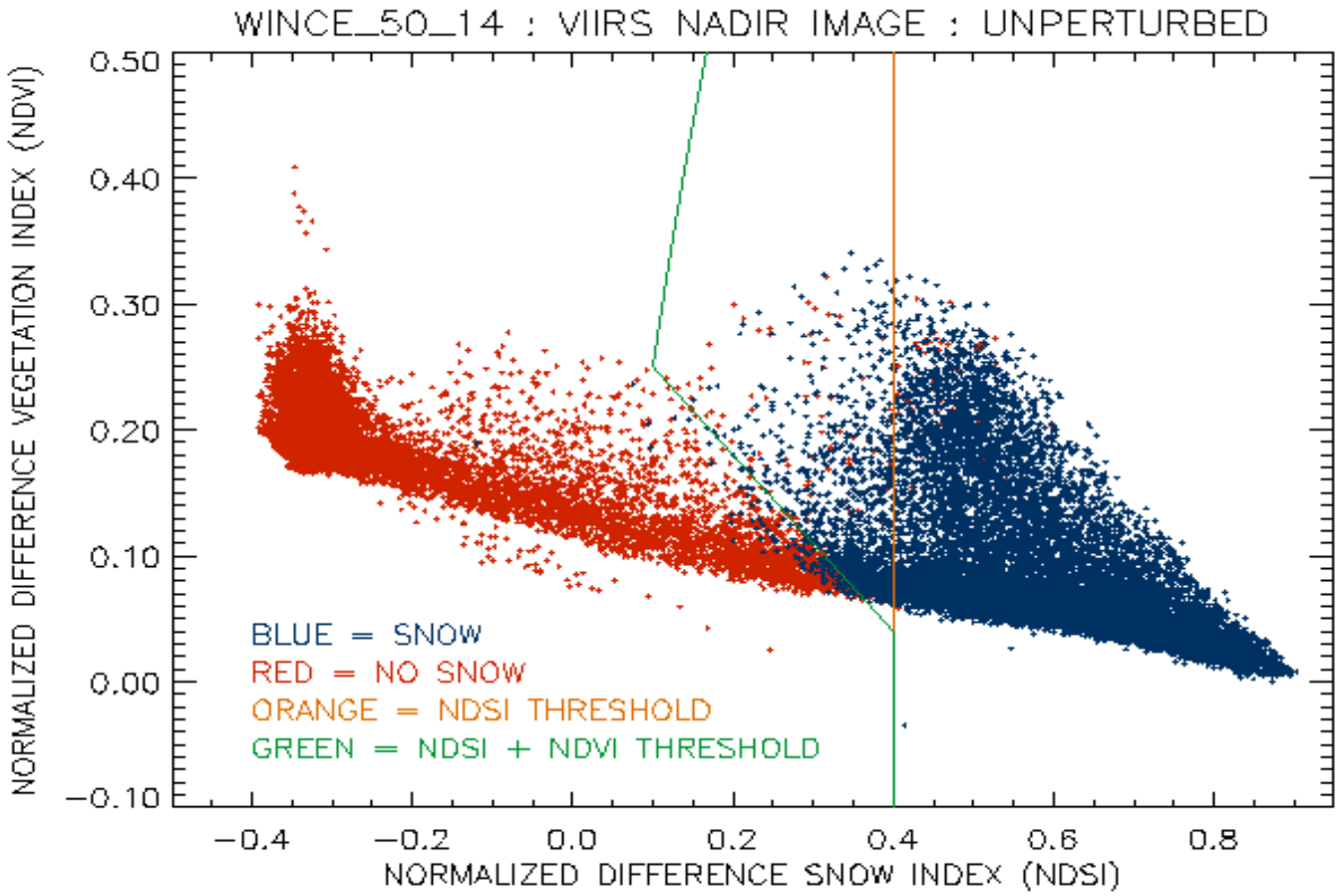

Figure 16: NDSI versus NDVI scatter plot of the MAS Colorado winter scene (WINCE_50_14). The image has been aggregated to a VIIRS pixel size at nadir.

Correct classification occurs when pixels classified as snow (blue) fall to the right of the green threshold boundary and when pixels classified as no snow (red) fall to the left of the boundary. Correct classification occurs for 98.52 % of the pixels. Without the NDVI correction, additional misclassification would occur where blue pixels fall to the left of the orange boundary.

Figure 17 shows an NDSI versus NDVI scatter plot for scene 1, aggregated to a VIIRS pixel size at nadir, with error perturbations (atmospheric correction, sensor noise, sensor MTF, band misregistration) added.

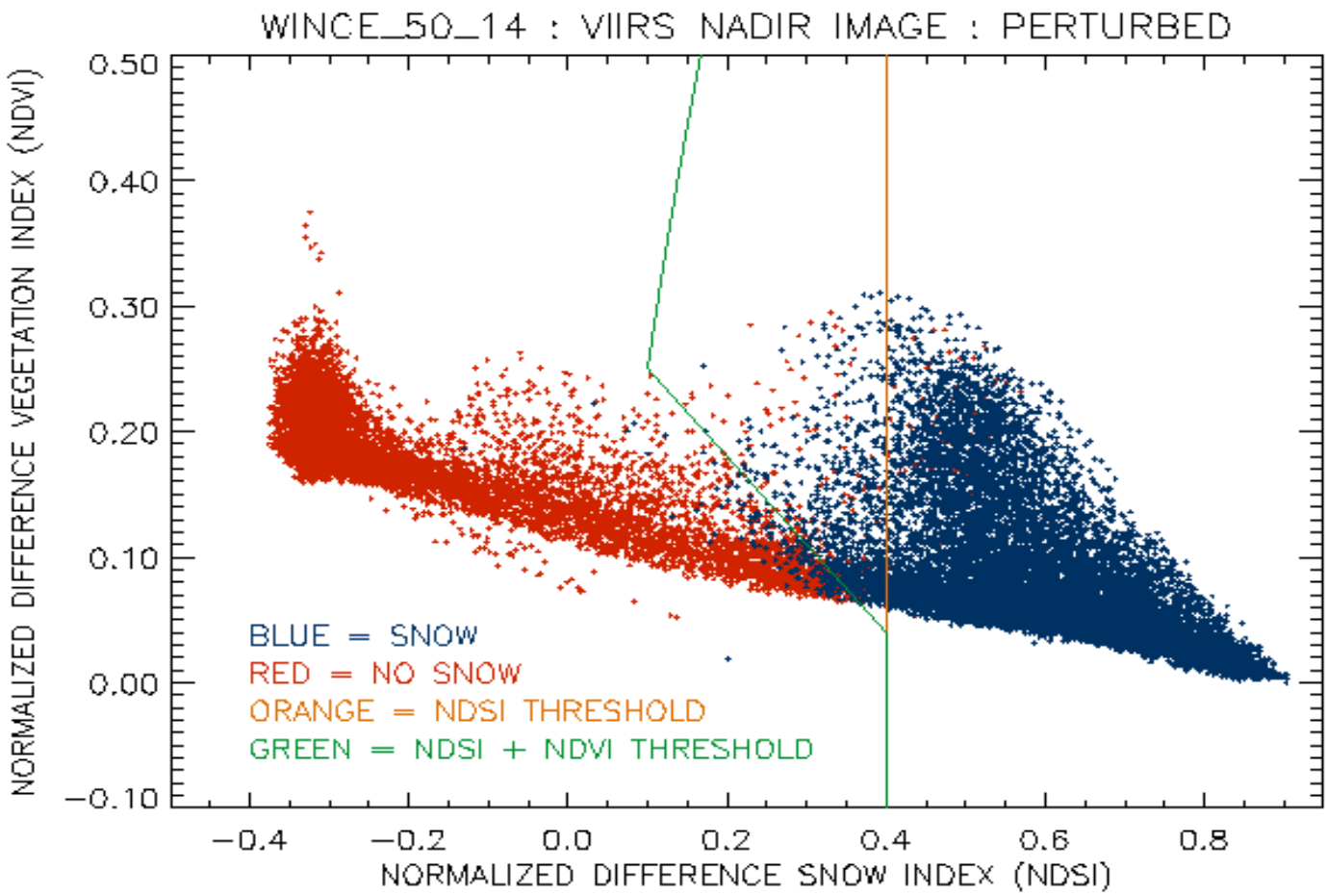

Figure 17: NDSI versus NDVI scatter plot the MAS Colorado winter scene (WINCE_50_14). The image has been aggregated to a VIIRS pixel size at nadir. Error perturbations have been added to the scene.

Correct classification occurs when pixels classified as snow (blue) fall to the right of the green threshold boundary and when pixels classified as no snow (red) fall to the left of the boundary. Correct classification occurs for 97.79 % of the pixels. Without the NDVI correction, additional misclassification would occur where blue pixels fall to the left of the orange boundary.

The probability of correct typing for scene 4 is illustrated as a function of snow fraction truth in Figure 18.

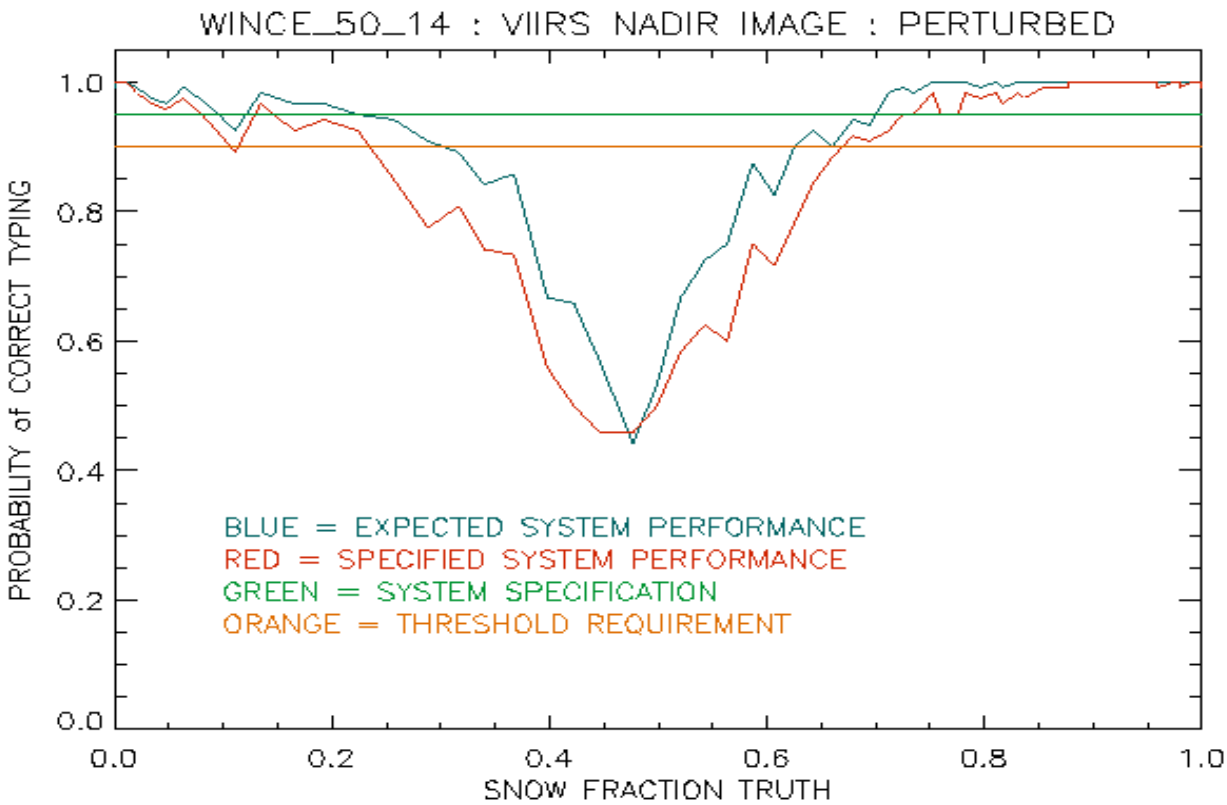

Figure 18: Probability of Correct Typing vs. Snow Fraction for the MAS Colorado winter scene (WINCE_50_14). The scene was aggregated to a pixel size of 0.4 km to simulate a VIIRS nadir view.

Results from the analysis of the Colorado mixed snow cover scene have been incorporated into a stratified performance summary, shown in Table 6.

Table 6. Snow Binary Map : Probability of Correct Typing (%)

Clear, Nadir, SZA = 60 degrees, Some Canopy, Mixed Snow/No Snow

	Snow Fraction (Truth)					**Fraction of Mixed Pixels**		
	0.0 – 0.2	0.2 – 0.4	0.4 – 0.6	0.6 – 0.8	0.8 – 1.0	10%	30%	50%
Specification	99.36	80.56	56.74	92.07	99.88	99.04	97.12	95.20
Performance	99.60	89.95	66.51	96.35	99.99	99.37	98.13	96.89

An explanation of the stratification bins is in Section 4.1.1. Probability of correct typing for each of the "truth" bins was derived by examining the classification error for the subset of pixels falling into the "truth" range of the given bin. Probability of correct typing for each of the "fraction of mixed pixels" bins was derived in the following manner. The probability of correct typing for pure pixels was calculated by examining the classification error for the subset of pure pixels. The probability of correct typing for mixed pixels was calculated by examining the classification error for the subset of mixed pixels. The probability of correct typing for a given fraction of mixed pixels is calculated as the weighted mean of the pure pixel and mixed pixel probabilities, with the mixed pixel weight equal to the fraction of mixed pixels.

It is important to note that the probability of correct typing for any binary classifier must approach 50% when the "truth" approaches 0.5. The performance results shown in Figure 18 and Table 6 reflect this characteristic. The practical measure of performance is for a realistic distribution of true fraction for various scenes, as is shown in the last three columns of Table 6.

4.2.1.1 Snow Binary Map Error Budgets

The various error sources have been incorporated into error budgets for easy, typical, and difficult cases. These are shown in Tables 7, 8 and 9.

Table 7. Error Budget for Retrieval of the Snow Binary Map EDR (Case 1)

SNOW COVER (Snow Binary Map) Case 1: Clear, Nadir, SZA = 60 degrees, 10% Mixed Pixels (Easy case)		
Specification v5 (CDR)	**Probability of Correct Typing (%)**	**Reference**
Threshold	90.00	VIIRS SRD
Objective	N/A	
System Specification	95.00	Raytheon VIIRS Specification v5
Predicted Performance	99.37	Raytheon VIIRS Specification v5
Margin	95.60	Raytheon VIIRS Specification v5
Algorithm Specification	99.55	Raytheon VIIRS Specification v5
Thresholds	99.58	Raytheon VIIRS Specification v5
Atmospheric Correction	99.98	Raytheon VIIRS Specification v5
Sensor Specification	99.81	Raytheon VIIRS Specification v5
Sensor Noise	99.96	Raytheon VIIRS Specification v5
MTF	99.84	Raytheon VIIRS Specification v5
Band Misregistration	99.85	Raytheon VIIRS Specification v5

Table 8. Error Budget for Retrieval of the Snow Binary Map EDR (Case 2)

SNOW COVER (Snow Binary Map) Case 2: Clear, Nadir, SZA = 60 degrees, 30% Mixed Pixels (Typical case)		
Specification v5 (CDR)	Probability of Correct Typing (%)	Reference
Threshold	90.00	VIIRS SRD
Objective	N/A	
System Specification	95.00	Raytheon VIIRS Specification v5
Predicted Performance	98.13	Raytheon VIIRS Specification v5
Margin	96.81	Raytheon VIIRS Specification v5
Algorithm Specification	98.67	Raytheon VIIRS Specification v5
Thresholds	98.74	Raytheon VIIRS Specification v5
Atmospheric Correction	99.93	Raytheon VIIRS Specification v5
Sensor Specification	99.43	Raytheon VIIRS Specification v5
Sensor Noise	99.89	Raytheon VIIRS Specification v5
MTF	99.52	Raytheon VIIRS Specification v5
Band Misregistration	99.55	Raytheon VIIRS Specification v5

Table 9. Error Budget for Retrieval of the Snow Binary Map EDR (Case 3)

SNOW COVER (Snow Binary Map) Case 3: Clear, Nadir, SZA = 60 degrees, 50% Mixed Pixels (Hard case)		
Specification v5 (CDR)	Probability of Correct Typing (%)	Reference
Threshold	90.00	VIIRS SRD
Objective	N/A	
System Specification	95.00	Raytheon VIIRS Specification v5
Predicted Performance	96.89	Raytheon VIIRS Specification v5
Margin	98.05	Raytheon VIIRS Specification v5
Algorithm Specification	97.80	Raytheon VIIRS Specification v5
Thresholds	97.91	Raytheon VIIRS Specification v5
Atmospheric Correction	99.89	Raytheon VIIRS Specification v5
Sensor Specification	99.04	Raytheon VIIRS Specification v5
Sensor Noise	99.82	Raytheon VIIRS Specification v5
MTF	99.20	Raytheon VIIRS Specification v5
Band Misregistration	99.25	Raytheon VIIRS Specification v5

If the various error sources listed in tables 7, 8, and 9 were completely uncorrelated, the combination of probabilities would follow the formula:

$$P = P_1 \times P_2 \times \ldots \times P_N$$

Because the various error sources contain some correlation, the probabilities do not combine in this way. To derive the error budgets, we used multiple simulated images. Each simulated image contained one and only one of the perturbations. Comparison of retrieval with truth for each of the simulations gave us the error contribution of the associated perturbation. To simulate the easy, typical, and difficult cases, we computed separate errors for pure pixels and mixed pixels, and weighted accordingly.

The largest error is the “thresholds” error. This error is caused by the limitations of our limited threshold tests in accounting for the real variety of surface and canopy reflectance. In principle, the error could be reduced by improvements in canopy modeling and by the use of different thresholds for different surface types. Because our performance is significantly better than the SRD requirement, we do not at present see the necessity to deviate from the MODIS approach.

Finally, we note that the sensor signal-to-noise performance is better than the specification. For the 1.6 micron band, the improvement is substantial. Because sensor noise is such a small component of the error budget, EDR performance would still meet specification if the sensor signal-to-noise were degraded to its specification values. For example, if we replace sensor noise performance with sensor noise specification, our probability of correct typing for our hard case degrades from to 96.88 % to 95.20 %, which meets our specification even for the hard case (c.f. Table 9).

4.2.2 Snow Fraction

Verification of the performance of the snow fraction algorithm is by analysis and simulation.

Errors in snow fraction are produced by errors in surface reflectance, model snow reflectance, and model non-snow reflectance, as can be seen from equation (3.3.3.3). Our flowdown studies suggest that spatial errors (MTF and band misregistration) are important for scenes where mixed snow cover is variable on spatial scales comparable to the horizontal cell size. To simulate these errors, we have analyzed MAS scenes of mixed snow cover.

For our error analysis, we have assumed equally weighted bands. Optimal band weighting can in principle reduce our errors.

Errors in Model Snow Reflectance: The algorithm selects the snow reflectance model which minimizes the RMS error. Deviation of the model spectrum from the “true” snow reflectance introduces error. We have performed simulations to quantify this error. We adopted 10 models of snow reflectance, ranging from grain sizes of 50 microns to 1000 microns. We selected a MAS scene of mixed snow cover and retrieved a snow/no snow classification for each MAS pixel, using the snow binary map algorithm. We aggregated the classified MAS pixels to VIIRS pixel sizes to obtain “true” snow fraction. For each MAS pixel classified as snow, we simulated 1000 “real” reflectance spectra by random interpolation between the models. That is, we assumed that the combination of a random fraction of each of the 10 types is an adequate model for “true” reflectance from the snow cover in a pixel. For each pixel classified as no snow, we used the observed reflectance. We

aggregated the reflectances to VIIRS pixel size and performed the snow fraction retrieval, using the 10 model snow spectra and the observed non-snow spectra. The RMS snow fraction measurement uncertainty was 0.02, computed by comparison of the retrieved snow fractions to the "true" snow fraction.

Errors in Model Non-Snow Reflectance: The non-snow reflectance will be obtained from the VIIRS Monthly Non-Snow Reflectance IP. This database will be initialized from MODIS data, and continually updated during the NPP and NPOESS missions. We have simulated the performance of the database by using the average observed non-snow spectrum in a 6 km cell surrounding a given pixel as a proxy. This produces an error of 0.04 in snow fraction. We adopt this error in our budget, but note that the quantification of this error source will require verification. Verification will require the MODIS data.

Errors in Surface Reflectance: We have obtained these from the performance analysis of the Surface Reflectance algorithm *[Y2411]*. The errors depend on surface reflectance truth, which is correlated with snow fraction. Reflectance errors were calculated for a solar zenith angle of 60 degrees, an aerosol optical thickness of 0.1, an error in aerosol optical thickness of 0.05, and a calibration bias of 2%, to simulate expected system performance for a typical solar zenith angle and atmosphere.

MTF Errors: Errors due to MTF smearing of the radiances have been analyzed. Our test scenes were MODIS Airborne Simulator scenes of mixed snow cover. Ground truth was determined at 50 meter spatial resolution. We adopted a sensor GIFOV of 1.3 km at 3000 km swath, subjected the scenes to an MTF smearing derived from the current VIIRS baseline sensor performance model, retrieved snow cover with our algorithm, and computed Measurement Uncertainty. For a scene with 50% mixed pixels, the error in snow fraction due to MTF was 0.064. We adopt a linear scaling of MTF error with fraction of mixed pixels, so that the estimated MTF error for scenes with 30% mixed pixels is 0.039.

Band Misregistration Errors: We applied a band misregistration of 0.2 pixels in cross track and along track directions, following the VIIRS system specification for band-band registration *[SS154640-001]*. For a scene with 50% mixed pixels, the error in snow fraction was 0.037. As with MTF, we adopt a linear scaling of error with fraction of mixed pixels, so that the estimated band misregistration error for scenes with 30% mixed pixels is 0.022.

Tables 10, 11, and 12 show the errors stratified by scan angle, and snow fraction truth for easy, typical, and hard cases.

Table 10. Snow Fraction Measurement Uncertainty : Clear, 10% Mixed Pixels (Easy case)

Scan Angle	**Snow Fraction (Truth)**			
	0.0 – 0.25	0.25 – 0.5	0.5 – 0.75	0.75 – 1.0
Nadir	.053	.056	.061	.067
Edge-of-Scan	.061	.065	.077	.091

Table 11. Snow Fraction Measurement Uncertainty : Clear, 30% Mixed Pixels (Typical case)

Scan Angle	**Snow Fraction (Truth)**			
	0.0 – 0.25	0.25 – 0.5	0.5 – 0.75	0.75 – 1.0
Nadir	.070	.072	.076	.081
Edge-of-Scan	.077	.079	.089	.102

Table 12. Snow Fraction Measurement Uncertainty : Clear, 50% Mixed Pixels (Hard Case)

Scan Angle	**Snow Fraction (Truth)**			
	0.0 – 0.25	0.25 – 0.5	0.5 – 0.75	0.75 – 1.0
Nadir	.096	.097	.100	.104
Edge-of-Scan	.100	.102	.110	.121

An explanation of the stratification bins is in Section 4.1.2.

4.2.2.1 Snow Fraction Error Budget

The various error sources for a typical case have been incorporated into an error budget, shown in Table 13.

Table 13. Error Budget for Retrieval of the Snow Fraction EDR

SNOW COVER (Snow Fraction) Case: Clear, Nadir, SZA = 60 degrees, 30% Mixed Pixels, Truth = 0.5		
Specification v5 (CDR)	Measurement Uncertainty	Reference
Threshold	N/A	
Objective	0.1000	VIIRS SRD
System Specification	0.1000	Raytheon VIIRS Specification v5
Predicted Performance	0.0738	Raytheon VIIRS Specification v5
Margin	0.0675	Raytheon VIIRS Specification v5
Algorithm Specification	0.0587	Raytheon VIIRS Specification v5
Surface Reflectance	0.0380	VIIRS Snow Cover ATBD v5
Snow Reflectance	0.0200	VIIRS Snow Cover ATBD v5
Non-Snow Reflectance	0.0400	VIIRS Snow Cover ATBD v5
Sensor Specification	0.0450	Raytheon VIIRS Specification v5
MTF	0.0390	VIIRS Snow Cover ATBD v5
Band Misregistration	0.0220	VIIRS Snow Cover ATBD v5

4.3 LIMITS OF APPLICABILITY

In this section, we discuss the conditions under which our EDR specified performance cannot be attained.

4.3.1 Cloudy

The VIIRS Snow Cover EDR is required under clear conditions only, with clear defined as a cloud optical thickness less than 0.03. Our specification is for clear scenes only. Clouds are not amenable to spectral mixture analysis, because their reflectance properties are highly variable. The standard approach to minimize errors caused by clouds is to mask pixels where clouds are likely to be present in the radiance path. The VIIRS Cloud Mask *[Y2412]* will perform this function. Because no cloud mask is perfect, there will be some source of error caused by the effects of unmasked clouds. Thin clouds will perturb the upwelling surface reflected radiance by absorption and scattering, and will also be a source of reflected and emitted radiance unrelated to the surface. There will also be error due to incorrect classification of cloud contaminated pixels as clear as well as due to cloud shadows.

It is desirable to perform tests to determine the expected size of the retrieval errors under various conditions of cloud optical thickness and phase. Thin cirrus clouds are a particularly important case of cloud error, because they are particularly difficult for the cloud mask to detect over snow. The conditions under which the specification can not be attained may include a range of cloud optical thickness. The range will be determined by a balance between the increasing effect of clouds on the signal and the increasing probability of correct masking. The specification of this range has been deferred to future validation activity.

4.3.2 Low Light or Nighttime

The algorithm requires solar reflectance. Thermal contrast between snow and non-snow land surfaces is not a characteristic property. A solar zenith angle threshold of 70 degrees is adopted. For larger angles, surface reflectance errors become too large to guarantee the specification. Improved atmospheric correction would allow us to increase this threshold. The extension and refinement of the threshold is a goal of pre-launch initialization. MODIS experience will be of great value. Note that the EDR will be reported for solar zenith angles of 70-85 degrees, with a quality flag attached. AOT and thin clouds could affect where the solar zenith angle thresholds are set (c.f. Section 3.3.5.2).

4.3.3 Forest canopy (snow fraction)

A large part of snow cover occurs in the boreal forests. These forests obscure most of the underlying surface. Observations of forest canopy under conditions where 100 percent snow cover is expected to show albedo variations as large as 70%. Snow cover measurement uncertainties of 10% are not possible under these conditions. We have to be able to identify and flag pixels of forest canopy. The binary snow map algorithm will perform in boreal forests. We have verified its performance for the winter forest canopy of Northern Minnesota. Its performance in the deeper boreal forests is TBD. MODIS validation is expected to thoroughly characterize the performance in boreal forests.

4.4 PRACTICAL CONSIDERATIONS

4.4.1 Numerical Computation Considerations

Paragraph SRDV3.2.1.5.4-1 of the VIIRS SRD states the following:

> "The scientific SDR and EDR algorithms delivered by the VIIRS contractor shall be convertible into operational code that is compatible with a 20 minute maximum processing time at either the DoD Centrals or DoD field terminals for the conversion of all pertinent RDRs into all required EDRs for the site or terminal, including those based wholly or in part on data from other sensor suites."

RDR here stands for Raw Data Record. This essentially means that any and all EDRs must be completely processed from VIIRS raw data, including calibration and geolocation, within 20 minutes from the time the raw data are available. This requirement is a strong reminder that VIIRS is an operational instrument.

For the snow Cover EDR, the challenges posed by the SRD time requirement are minimal. The algorithm does not involve any kind of iteration or inversion of physically based models. The spectral unmixing method we use is not time intensive, as it reduces to a fixed number of tie point calculations with a single decision node.

4.4.2 Programming and Procedural Considerations

VIIRS Phase II efforts are largely software-focused, and the methodology for this development work is based on sound and proven principles, as discussed in the VIIRS Algorithm Software Development Plan *[Y6635]*.

The present maturity of the VIIRS software is detailed in the VIIRS Algorithm Software Maturity Assessment document *[Y6661]*. The maturity and remaining Phase II tasks for the algorithms themselves is summarized in the VIIRS Algorithm/Data Processing Technical Report *[Y7040]*.

All procedures are automatic, to perform in the operational environment. The Snow Cover EDR will be produced in an integrated software system within the VIIRS Ground Segment of the IDPS. The algorithm is implemented by an independent testable software unit. The software design relevant to this unit is summarized in the VIIRS Context Level Software Architecture *[Y2469]*, Snow Ice Module Level Software Architecture *[Y2477]*, and Snow Cover Unit Level Detailed Design *[Y3234]*. The design will be tested at the system level as described in the most recent versions of the VIIRS Software Integration and Test Plan *[Y3236]*, Algorithm Verification and Validation Plan *[Y3237]*, and System Verification and Validation Plan *[Y3270]*. A summary of the ultimate strategy for operational application of the system of VIIRS algorithms is provided in the VIIRS Operations Concept document *[Y2468]*. The VIIRS Interface Control Document (ICD *[Y2470]*) provides more detail on the specifics of ancillary data requirements for VIIRS EDR products.

4.4.3 Configuration of Retrievals

The algorithm requires the availability of input data from a variety of sources, including VIIRS SDRs, VIIRS IPs, and a number of LUTs. A detailed list of these sources can be found in the Snow Ice Module Level Software Architecture *[Y2477]* and Snow Cover Unit Level Detailed Design *[Y3234]*. The EDR output is used as input to the Surface Reflectance and Surface Type algorithms in the VIIRS system. The NPOESS/VIIRS processing configuration is designed to satisfy these expectations *[Y2469]*.

4.4.4 Quality Assessment and Diagnostics

Quality flags will be attached to each imagery resolution pixel and each moderate resolution pixel. The snow fraction algorithm will produce an error estimate for each pixel. The algorithm should be expected to archive the final pixel errors for quality assessment. Ideally, a pixel error greater than an accepted threshold will be flagged. A description of the quality flags can be found in the Snow Cover Unit Level Detailed Design *[Y3234]*.

4.4.5 Exception Handling

The software is designed to handle a wide variety of processing problems, including bad and missing data and fatal errors. In the event that processing problems prevent the production of useful EDR data, error flag information will be written to the output EDR file as metadata. A detailed description can be found in the Snow Cover Unit Level Detailed Design *[Y3234]*.

4.5 VALIDATION

Validation of the Snow Cover EDR will be conducted as part of the VIIRS System Verification and Validation Plan *[Y3270]*. It will benefit greatly from MODIS data and MODIS validation experience.

MODIS-derived snow maps are compared with snow cover maps generated by NOAA from the IMS. The techniques used by NOAA and the snow and ice data sets they generate are used for validation of MODIS snow products. Close collaboration between the NASA/GSFC and NOAA/NESDIS groups is maintained for exchange of ideas and algorithms for snow cover mapping and validation. NOAA/NOHRSC snow cover maps are also used for MODIS validation purposes and NASA/GSFC communication with the NOHRSC is maintained. Our plan is to establish and maintain communication with the NOAA and NASA snow groups during the pre-launch phase.

In addition, comparisons will be made between MODIS maps and maps derived from Scanning Multichannel Microwave Imager (SSM/I) data, if available, or Advanced Microwave Scanning Radiometer (AMSR) data after the launch of the first EOS-Aqua platform in 2002. Comparison of Snowmap results with these independently-produced snow data sets will allow errors to be identified that will permit us to determine the accuracy of the global maps relative to one another.

Radiative transfer models will be applied to large solar zenith angle data to optimize the models for low sun conditions. MODIS data taken at solar zenith angles greater than 70 degrees will be studied to assist in determining the band weighting functions. The limiting factor is believed to be the reliability of atmospheric correction at larger solar zenith angles. Plane parallel radiative transfer algorithms are inaccurate for angles greater than 70-75 degrees. Development of improved radiative transfer models at larger angles will allow us to relax this constraint. To solve the Radiative Transfer Equation appropriately one would have to take into account the spherical shell atmosphere geometry (Thomas and Stamnes, 1998). It is expected that “truth” can be established from *in situ* data obtained from MODIS validation campaigns. Discrete Ordinates Radiative Transfer (DISORT) models are currently being used to validate the MODIS snow products (Nolin and Stroeve, 2000). These models can be incorporated into our VIIRS look up tables during the initialization phase.

The pre-launch plan includes sensitivity studies, analysis of simulated VIIRS data, and verification using MODIS data. Our plan is to maintain close contact with the MODIS teams to coordinate our initialization activity with their post-launch validation. Observations from AVIRIS, MAS, Landsat ETM+, MODIS, GLI, and NPP/VIIRS will be used in the pre-launch phase to study the error characteristics and optimum techniques for the algorithm. It is expected that MODIS validation data will be of great value. MODIS/AMSR data can be used to investigate prospects for VIIRS/CMIS data fusion, and for cross-validation of the Vis/IR algorithm. The NPP/VIIRS will be critical in adjusting and verifying the values of the parameters in our LUTs. This process will be essential in making the algorithm operational prior to the NPOESS mission. We recommend an NPP/VIIRS validation campaign that includes *in situ* field measurements, ER-2 underflights (AVIRIS and MAS), and low level aircraft measurements at spatial resolutions as fine as 10 meters (e.g. RC-10 camera data). NPP/VIIRS data can be re-processed many times with various combinations of band weight functions and reflectance thresholds, and resulting snow retrievals can be compared to “truth” established from the auxiliary data. In this way, optimum band weight functions and reflectance thresholds can be selected.

Plans include the development of a reliable global reference database of non-snow endmembers. The development the database will be an ongoing project. We expect the MODIS and NPP missions to accumulate information on surface constituents and their reflectance spectra for various global locations and times of year.

A MODIS Surface Reflectance product (Vermote, 1999) is expected to be stored at the MODIS Distributed Active Archive Center (DAAC). The product will contain the surface reflectances, corrected for atmosphere and BRDF, for MODIS bands 1 and 2 at 250 meter resolution, and bands 3-7 at 500 meter resolution. This database should be more than sufficient to establish a monthly mean non-snow reflectance database for VIIRS at a fixed latitude/longitude grid of 1 km. We expect the global coverage by MODIS on the Terra and Aqua platforms will provide sufficient directional information to allow for directional reflectance correction.

We will create a global database of monthly mean non-snow reflectance in the MODIS reflectance bands from MODIS data. The reflectances will be corrected to VIIRS bands by spectral interpolation. The corrected database will be used at the start of the NPP mission. As the NPP mission proceeds, the database will be continually updated from NPP observations. We expect a smooth transition from MODIS to NPP to NPOESS.

We will also extend our library of snow reflectance spectra. Our current (JHU) library covers a limited set of snow grain sizes, but does not account for the effects of impurities. It is expected that the capabilities of the planned Global Imager (GLI) mission will provide useful data for this activity.

Our plan is designed to interface smoothly with post-launch validation activity. The availability of NPP/VIIRS data prior to the NPOESS mission will be of enormous benefit. We would propose to conduct an NPP/VIIRS validation campaign similar to the MODIS validation activity, and use it as a model for the post-launch NPOESS/VIIRS validation campaign. In this sense, post-launch validation will already have been simulated by the pre-launch validation activity. Following launch, we would substitute real VIIRS data for the pre-launch simulated data. Cross-validation with NPOESS/CMIS provide a valuable extra capability.

5.0 ASSUMPTIONS

The statements and conclusions in this document are subject to the validity of the following assumptions.

1. An effective cloud mask over snow and ice surfaces will be available from the VIIRS Cloud Mask algorithm *[Y2412]*.

2. Surface reflectance will be derived from TOA radiances by the Surface Reflectance algorithm, with errors as specified in the Surface Reflectance ATBD *[Y2411]*.

3. Pixels subject to large forest canopy errors can be identified and flagged.

4. Non-snow reflectance will initially be available from an external global database. The creation of this database is a required initialization activity.

5. Snow and non-snow directional reflectance corrections will be available from look up tables. The generation of these look up tables is a required initialization activity.

6.0 REFERENCES

Ackerman, S. *et al.* (1997). Discriminating clear sky from cloud with MODIS. 1997.ATBD MOD-06. *http://eospso.gsfc.nasa.gov/atbd/modistables.html*

Barton, J.S., D.K. Hall and G.A. Riggs, (2000). "Remote sensing of fractional snow cover using Moderate Resolution Imaging Spectroradiometer (MODIS) data," *Proceedings of the 57th Eastern Snow Conference, 18-19 May 2000, Syracuse, NY,* in press.

Barton, J.S., D.K. Hall, and G.A. Riggs, (2001). "Thermal and geometric thresholds in the mapping of snow with MODIS.", draft (http://modis-snow-ice.gsfc.nasa.gov/pap_therm.html)

Bohren, C.F., and B.R. Barkstrom (1974). Theory of the optical properties of snow. *J. Geophys. Res.*, 79, 4527-4535.

Bromwich, D.H. and R.-Y. Tzeng (1994). Simulation of the modern arctic climate by the NCAR CCM1. *J. Climate***,** 7, 1050-1069.

Carroll, T.R., J.V. Baglio, Jr., J.P. Verdin, and E.W. Holroyd, III (1989). Operational mapping of snow cover in the United States and Canada, using airborne and satellite data. *Proceedings of the 12th Canadian Symposium on Remote Sensing*, V. 3, IGARSS '89, 10-14 July 1989, Vancouver, Canada.

Carroll, T.R., (1990). Operational airborne and satellite snow cover products of the National Operational Hydrologic Remote Sensing Center. *Proceedings of the 47th annual Eastern Snow Conference*, June 7-8, 1990, Bangor, Maine, CRREL Special Report 90-44.

Chang, A.T.C. (1998). AMSR-based SWE retrieval algorithm ATBD. *http://wwwghcc.msfc.nasa.gov/AMSR/snow_ATBD*

Chang, A.T.C., J.L. Foster and D.K. Hall, (1987). Microwave snow signatures (1.5 mm to 3 cm) over Alaska, *Cold Regions Science and Technology*, 13, pp 153-160.

Chang, A.T.C. *et al.* (1987). Estimating snowpack parameters in the Colorado River basin. International Association of Hydrological Sciences Publication 166 (Symposium at Vancouver 1987 – *Large Scale Effects of Seasonal Snow Cover*), 343-352.

Crane, R.G. and M.R. Anderson (1984). Satellite discrimination of snow/cloud surfaces. *Intl. J. Remote Sens*., 5(1), 213-223.

Dozier, J., S.R. Schneider and D.F. McGinnis Jr., 1981: Effect of grain size and snowpack water equivalence on visible and near-infrared satellite observations of snow. *Water Resources Research*, 17, pp 1213-1221.

Dozier, J. (1984). Snow reflectance from Landsat-4 Thematic Mapper. *IEEE Trans. Geosci. Remote Sens.*, 22(3), 323-328.

Dozier, J. (1989). Spectral signature of alpine snow cover from the Landsat Thematic Mapper. *Remote Sens. Environ.*, 28, 9-22.

Foster, J.L., D.K. Hall, A.T.C. Chang and A. Rango, 1984: An overview of passive microwave snow research and results, *Reviews of Geophysics*, 22, pp 195-208.

Foster, J.L., and A.T.C. Chang (1993). Snow cover. In *Atlas of Satellite Observations Related to Global Change* R.J. Gurney, C.L. Parkinson, and J.L. Foster (eds.), Cambridge University Press, Cambridge, pp. 361-370.

Foster, J.L., A.T.C. Chang, and D.K. Hall (1997). Comparison of snow mass estimates from a prototype passive microwave snow algorithm, a revised algorithm, and a snow depth climatology. *Remote Sens. Environ.*, 62, 132-142.

Grenfell, T.C., D.K. Perovich, and J.A. Ogren (1981). Spectral albedos of an alpine snowpack. *Cold Regions Sci. Technol*., 4, 121-127.

Grody, N.C., and A.N. Basist (1996). Global identification of snow cover using SSM/I instruments. *IEEE Trans. Geosci. Remote Sens.*, 34(1), 237-249.

Hall, D.K., A.Tait, G. Riggs, and V. Salomonson (1998). MODIS: Snow mapping Algorithm and the Sea Ice Mapping Algorithm (Version 4.0). ATBD-MOD-10. *http://eospso.gsfc.nasa.gov/atbd/modistables.html*

Hall, D.K., et al. (2001a). Algorithm Theoretical Basis Document (ATBD) for the MODIS Snow and Sea Ice-Mapping Algorithms. http://snowmelt.gsfc.nasa.gov/MODIS_Snow/atbd01.html

Hall, D.K., R.E.J. Kelly, G.A. Riggs, A.T.C. Chang and J.L. Foster, (2001b). "Assessment of the relative accuracy of hemispheric-scale snow-cover maps," *Annals of Glaciology*, V.34, in press.

Hall, D.K., G.A. Riggs, V.V. Salomonson, N. DiGiromamo and K.J. Bayr, (2001c). "MODIS Snow Cover Products," *Remote Sensing of Environment*, in press.

Hall, D.K., J.L. Foster, V.V. Salomonson, A.G. Klein and J.Y.L. Chien, (2001d). "Development of a Technique to Assess Snow-Cover Mapping Errors from Space," *IEEE Transactions on Geoscience and Remote Sensing*, 39(2).

Hoffer, R.M. (1978). Biological and physical considerations in applying computer-aided analysis techniques to remote sensor data. In *Remote Sensing: The Quantitative Approach* (P.H. Swain and S.M. Davis, eds.). New York: McGraw-Hill.

Klein,A.G., D.K. Hall, and G.A. Riggs (1998). Improving snow-cover mapping in forests through the use of a canopy reflectance model. *Hydrological Processes*, 12(10-11): 1723-1744.

Klein, A.G., D.K. Hall and A. Nolin, 2001: Development of a prototype snow albedo algorithm for the NASA MODIS instrument, Proceedings of the 57th Eastern Snow Conference, 17-19 May 2000, Syracuse, NY.

Klein, A.G. (2001). "Development of a Prototype Snow Albedo Algorithm for the NASA MODIS Instrument," *Hydrological Processes*, submitted.

Matson, M., (1991). NOAA satellite snow cover data. *Palaeogeography, Palaeoclimatology, Palaeoecology*, 90: 213-218.

Matson, M., C.F. Roeplewski, and M.S. Varnadore (1986*). An Atlas of Satellite Derived Northern Hemisphere Snow Cover Frequency.* National Weather Service, Washington, D.C. 75pp.

Nolin, A.W., J. Dozier, and L.A.K. Mertes (1993). Mapping alpine snow using a spectral mixture modeling technique. *Annals of Glaciology*, 17, 121-124.

Nolin, A. W., and J. C. Stroeve (2000). Validation studies and sensitivity analyses for retrieval of snow albedo from EOS AM-1 instruments: Progress report for 1999-2000 work. May 20,2000, http://www-nsidc.colorado.edu/PROJECTS/ALBEDO

Nolin, A.W., and Liang (2000). *Remote Sensing Reviews*, 18, 307.

Painter, T.H., D.A. Roberts, R.O. Green, and J. Dozier (1998). The effect of grain size on spectral mixture analysis of snow covered area from AVIRIS data. *Remote Sens. of Environ.*, 65(3): 320-332.

Planet, W.G. (ed.), (1988). Data extraction and calibration of TIROS-N/NOAA radiometers. NOAA Technical Memorandum NESS 107 – Rev. 1, Oct. 1988. 130 pp.

Ramsay, B., 1998: The interactive multisensor snow and ice mapping system, *Hydrological Processes*, 12:1537-1546.

Rango, A., 1993: Snow hydrology processes and remote sensing, Hydrological Processes, 7:121-138.

Rango, A. and J. Martinec, 1982: Snow accumulation derived from modified depletion curves of snow coverage, Symposium on Hydrological Aspects of Alpine and High Mountain Areas, IAHS Publication No. 138:83-90.

Roberts, D.A., M.Gardner, R. Church, S. Ustin, G. Scheer, and R.O. Green (1998). Mapping Chaparral in the Santa Monica Mountains Using Multiple Endmember Spectral Mixture Models. *Remote Sens. of Environ.*, 65(3): 267-279.

Rosenthal, W.C. (1993). Mapping mountain snow cover at subpixel resolution from the Landsat Thematic Mapper. Master's thesis, Univ. Calif. at Santa Barbara.

Rosenthal, W.C., and J. Dozier (1996). Automated mapping of mountain snow cover at subpixel resolution from the Landsat TM. *Water Resources Res.*, 31(1), 115-130.

Thomas, G., and K. Stamnes (1998). Radiative transfer in the atmosphere and ocean. Textbook, Cambridge Atmospheric and Space Sciences Series.

Vermote, E. (1999). MODIS: Atmospheric Correction Algorithm Spectral Reflectances, ATBD-MOD-08. *http://eospso.gsfc.nasa.gov/atbd/modistables.html*

Warren, S.G. (1982). Optical properties of snow. *Rev. Geophys. Space Phys*., 20(1), 67-89.

Warren, S.G., and W.J.Wiscombe (1980). A model for the spectral albedo of snow. II. Snow containing atmospheric aerosols, *J. Atmos. Sci.*, 37(12), 2734-2745.

Winther, J.G., 1992: Landsat thematic mapper (TM) derived reflectance from a mountainous watershed during the snow melt season, *Nordic Hydrology*, 23, pp 273-290.

Wiscombe, W.J., and S.G. Warren (1980). A model for the spectral albedo of snow,1,pure snow. *J. Atmos. Sci.*, 37(12), 2712-2733.